Variation in the Permeability of Rocks due to Transient Disturbances in Axial Stress or Pore Pressure

Sophea BOEUT

A thesis submitted in partial fulfillment of the requirements for the degree of Doctor of Engineering

Supervisor: Prof. Dr. Yoshiaki FUJII

Rock Mechanics Laboratory

Division of Sustainable Resources Engineering

Graduate School of Engineering

Hokkaido University

March 2020

Variation in the Permeability of Rocks due to Transient Disturbances in Axial Stress or Pore Pressure

Sophea BOEUT

Rock Mechanics Laboratory

Division of Sustainable Resources Engineering

Graduate School of Engineering

Hokkaido University

ABSTRACT

Large earthquakes can lead to persistent variations in the groundwater level in the near field. This would be due to the persistent variations in the permeability of the rock mass by permanent change in the strain through fault movement. These persistent variations in the groundwater levels may occur in the intermediate and even in the far fields which cannot be explained by variation in permeability associated with change in strain caused by fault movement because the change in strain is transient in the intermediate and far fields. The persistent variation in the permeability of rock mass caused by transient stress disturbances by earthquakes, if it exists, could explain not only the variation in groundwater level but also increase in petroleum production due to artificial vibrations, induction of small earthquakes by seismic waves, etc. in intermediate and far fields. However, it has not been verified whether the transient stress disturbances induce a persistent increase or decrease in the rock permeability.

To clarify the effects of transient stress disturbances on rock permeability, the study of three rock types, Kushiro Cretaceous sandstone, Shikotsu welded tuff, and Inada granite were carried out. The permeability values of intact and triaxially fractured Kushirio Cretaceous sandstone and Shikotsu welded tuff were measured before and after transient axial stress or pore pressure disturbances; the permeability of triaxially fractured Inada granite was measured under multiple transient disturbances in axial stress.

The permeability of the Kushiro Cretaceous sandstone decreased at zero stress disturbances. For the intact rocks, the permeability was kept almost constant with the disturbance amplitude. For the fractured rocks, the reductions became larger as the disturbance amplitudes increased. Regarding the pore pressure disturbances, the reductions in permeability of the intact rocks decreased as the pore pressure disturbances increased, whereas the reductions increased as the disturbance amplitudes increased for the fractured rocks.

For the Shikotsu welded tuff, the permeability decreased by fracturing. However, the change by the disturbances was small for all conditions.

The permeability of fractured Inada granite decreased with time in the tests. However, the permeability increased with each series of axial stress disturbances for amplitudes of 3 MPa or larger. The degree of increase in permeability increased with the axial stress disturbance amplitudes. The increased permeability decreased with time and recovered to its value before the disturbances. The time of recovery was longer for larger axial stress disturbance amplitudes.

The stress disturbances showed either decreasing or increasing effects on the permeability depending on the rock type and experimental conditions as stated above. However, when focusing on the fractured rocks which would be more important in field applications rather than the intact rocks, the argillaceous Kushiro Cretaceous sandstone mainly exhibited decreasing effects. The effects were mainly due to the closure of the rupture planes and the clogging of flow pathways by fine particles. In contrast, the glassy Shikotsu welded tuff showed small change. This would be because there were a lot of water flow paths in crushed glassy matrix. Permeability may not change even some flow paths were opened/closed or clogged/unclogged. The crystalline Inada granite mainly exhibited increase in permeability. The effects were mainly due to the opening of the apertures propped by hard fine particles, the enhancement of new microcracks, and unclogging of the fines from the flow pathways.

Variations in permeability due to transient stress disturbances have already been employed in seismic enhanced oil recovery (EOR) technique expecting an increase in permeability due to the movement of entrapped fluid in the reservoir. It could also be used for evaluation of the change in sealing ability of nuclear waste disposal caverns, and further employed to enhance natural gas recovery, to reroute underground water flow for various purposes, to prevent large earthquakes by inducing many small earthquakes, etc. in the future.

CONTENTS Page No.

	Abstract	**ii**
	List of Figures	**vi**
	List of Tables	**ix**
1.	Introduction	**1-5**
1.1	Background	2
1.2	Statement of the problem and objectives of the study	3
1.3	Outline of the research	4
2.	Experiment on Kushiro Cretaceous sandstone	**6-18**
2.1	Rock sample	7
2.2	Sample preparation and experimental setup	8
2.3	Experimental procedure and conditions	9
2.4	Results and discussions	12
	2.4.1 Transient disturbances in axial stress	12
	2.4.2 Transient disturbances in pore pressure	16
3.	Experiment on Shikotsu welded tuff	**19-28**
3.1	Rock sample	20
3.2	Sample preparation and experimental setup	21
3.3	Experimental procedure and conditions	21
3.4	Results and discussions	23
	3.4.1 Transient disturbances in axial stress	24
	3.4.2 Transient disturbances in pore pressure	26
4.	Experiment on Inada granite	**29-39**
4.1	Rock sample	30
4.2	Sample preparation and experimental setup	30
4.3	Experimental procedure and conditions	31
4.4	Results	32
4.5	Discussions	38
5.	Effects of transient stress disturbances on permeability	**40-42**

6. Concluding remarks **43-45**

Acknowledgement 46

References 47

List of Figures

1.1 Effects of earthquakes to underground properties..... 3

2.1 Location of gas wells for Cretaceous rock mass at Kushiro Coal Mine..... 7

2.2 Microscopic images of the Kushiro Cretaceous sandstone..... 7

2.3 (a) Cores of Kushiro Cretaceous sandstone and (b) Specimen coring..... 9

2.4 The permeability measurement apparatus..... 9

2.5 Experimental procedure..... 10

2.6 (a) Stress–strain curves and (b) maximum stress (σ_{max}) vs. the amplitudes of the axial stress disturbances ($\Delta\sigma_A$) under P_C = 10 MPa of the Kushiro Cretaceous sandstone..... 13

2.7 Variation in permeability in each hydrostatic stress state (Hold-1, Hold-2, Hold-3, and Hold-4) at the time of axial stress disturbance for the entire experiment: (a) AS-KCS2, (b) AS-KCS5, (c) AS-KCS8, and (d) AS-KCS9. Dist. 1 and Dist. 2 are the disturbances in prefailure and postfailure..... 14

2.8 Variation in permeability in each hydrostatic stress state at the time of axial stress disturbances and triaxial compression..... 14

2.9 Permeability ratio vs. (a) axial stress disturbance amplitude and (b) confining pressure of the intact rocks. The outlier data point was ignored for the regression analysis..... 15

2.10 Permeability ratio vs. (a) axial stress disturbance amplitude and (b) confining pressure of the fractured rocks..... 15

2.11 A specimen after an experiment (Pp-KCS3): (a) specimen showing the rupture plane, (b) gouge along the rupture plane, (c) microscopic image of the particles along the rupture plane, and (d) clogging and unclogging of an aperture by particles..... 15

2.12 (a) Stress–strain curves and (b) maximum stress (σ_{max}) vs. amplitudes of the pore pressure disturbances (ΔP_P) of the Kushiro Cretaceous sandstone..... 16

2.13 Variation in permeability in each hydrostatic stress state (Hold-1, Hold-2, Hold-3, and Hold-4) at the time of transient pore stress disturbances for the whole experiment: (a) P_P-KCS1, (b) P_P-KCS4, (c) P_P-KCS6, and (d) P_P-KCS7. Dist. 1 and Dist. 2 are the disturbances in prefailure and postfailure, respectively..... 17

2.14 Permeability variation due to pore pressure disturbances and triaxial compression under P_C = 10 MPa..... 17

2.15 Effect of pore pressure disturbances on the permeability ratio of the Kushiro Cretaceous sandstone, (a) intact rocks and (b) fractured rocks..... 18

3.1 Microscopic images of the Shikotsu welded tuff. Pl: plagioclase, Hb: amphibole, Cpx: clinopyroxene, IP: intergranular pore, PM: pumice, GI: glass, MS: mudstone, Vp: vesiculated pore..... 20

3.2 Specimen from block of Shikotsu welded tuff. (a) Measuring P-wave velocity of the block (b) coring direction and core specimen 21

3.3 Experimental procedure for the Shikotsu welded tuff..... 22

3.4 (a) Stress–strain curves and (b) maximum stress (σ_{max}) vs. amplitude of the axial stress disturbances ($\Delta\sigma_A$) of the Shikotsu welded tuff..... 25

3.5 (a) Stress–strain curves and (b) maximum stress (σ_{max}) vs. the amplitude of the pore pressure disturbance (ΔP_P) of the Shikotsu welded tuff..... 25

3.6 (a) Variation in permeability, and permeability ratios of the intact rocks (b) and fractured rocks (c) (P_P = 0.5 MPa) due to transient axial stress disturbances and triaxial compression of the Shikotsu welded tuff..... 25

3.7 (a) Variation in permeability, and permeability ratios of the intact rocks (b) and fractured rocks (c) (P_P = 0.1 MPa) due to transient axial stress disturbances and the triaxial compression of the Shikotsu welded tuff..... 26

3.8 (a) Variation in permeability and permeability ratios of the intact rocks (b) or fractured rocks (c) (P_P = 0.5 MPa) due to transient pore pressure disturbances and triaxial compression of the Shikotsu welded tuff..... 27

3.9 (a) Variation in permeability and permeability ratios of the intact rocks (b) and the fractured rocks (c) due to transient pore pressure disturbances and triaxial compression of the Shikotsu welded tuff (P_P = 0.1 MPa)..... 27

3.10 Images of blue resin impregnated thin-section samples after the tests under (a) $\Delta\sigma_A$ = 8 MPa, P_C = 5 MPa, P_P = 0.5 MPa, and (b) ΔP_P = 0.8 MPa, P_C = 5 MPa, P_P = 0.5 MPa. Left: original images, middle: processed images to emphasize the blue resin, and right: 28

magnified images.....

3.11 Effect of pore pressure on permeability ratios without stress disturbances..... 28

4.1 Microscopic images of Inada granite. Qz: Quartz, Pl: plagioclase, Kf: potash feldspar, Bi: biotite..... 30

4.2 Experimental procedure..... 31

4.3 Stress–strain curves..... 33

4.4 Variations in (a) axial stress and (b) water flow rate with time (IG-4, moving average of Dist.1 for 3 s)..... 33

4.5 Variations in axial strain during Hold-1-4: (a) IG-1, (b) IG-2, (c) IG-3, (d) IG-4, (e) IG-5, (f) IG-6, and (g) IG-7..... 34

4.6 Variations in permeability due to multiple transient axial stress disturbances: (a) IG-1, (b) IG-2, (c) IG-3, (d) IG-4, (e) IG-5, (g) IG-6, and (f) IG-7..... 35

4.7 Definition of k_n, k'_n, and Δt..... 36

4.8 Effects of axial stress disturbance amplitudes on (a) permeability ratio k'_4/k_1, (b) ratio of permeability after axial stress disturbances (k_n) to that before the disturbances (k'_n), and (c) time of decrease to the level before the disturbances (k_n to k'_{n-1}) 36

4.9 Specimens after the experiment: (a) IG-1, (b) IG-2, (c) IG-3, (d) IG-4, (e) IG-5, (f) IG-6, and (g) IG-7..... 37

4.10 (a) Gouge between the rupture planes after sieving (IG-4). (b) Gouge under microscope (IG-4). (c) Particle size distribution of gouge for IG-1, IG-4, and IG-6..... 38

4.11 Ratio of ultrasonic velocity of tested specimens to that before the test, *K*..... 38

List of Tables

1.1 The experimental conditions and the effect of stress disturbances on the permeability..... 4

2.1 Mineral composition of the Kushiro Cretaceous sandstone from XRD analysis..... 8

2.2 Physical properties of the rock samples shown as the average value (number of specimens) ± standard deviation..... 8

2.3 Experimental conditions for the Kushiro Cretaceous sandstone..... 11

3.1 Physical properties of the rock samples shown as the average value (number of specimens) ± standard deviation..... 20

3.2 Experimental condition for the Shikotsu welded tuff..... 23

4.1 Mineral composition and grain sizes of Inada granite..... 30

4.2 Experimental conditions under multi axial stress disturbances..... 32

5.1 Summary of the variations in permeability of the Kushiro Cretaceous sandstone..... 41

5.2 Summary of the variations in permeability of the Shikotsu welded tuff..... 42

1. Introduction

		Page No.
1.1	**Background**	**2-3**
1.2	**Statement of the problem and objectives of the study**	**3-4**
1.3	**Outline of the research**	**4-5**

1.1 Background

Large earthquakes can lead to persistent variations in the groundwater level in the near field (within the fault length) (Fig. 1.1a) (Bower & Heaton, 1978; Gudmundsson, 2000; Jonssson et al., 2003; Wang & Chia, 2008; Orihara et al., 2011; Lai et al., 2016). This would be a result of persistent variations in the permeability of the rock mass due to permanent change in the strain through fault movement. Such variations may also occur in an intermediate field (from one to several fault lengths) (Roeloffs, 1998; Kitagawa et al., 2006; Fujii et al., 2018a). However, previous studies reported that these persistent variation in the groundwater level may even occur in the far field (many fault lengths), up to thousands of kilometers from the epicenter (Fig. 1.1b) (Brodsky et al., 2003; Elkhoury et al., 2006; Liu & Manga, 2009; Manga et al., 2012; Manga & Wang, 2015).

Persistent variations in the groundwater level in the far field cannot be explained by variation in permeability associated with change in strain due to fault movement because change in strain is transient in the far field. Manga et al. (2012) suggested that persistent variations in the groundwater level could be due to a persistent increase in rock mass permeability as a result of transient stress disturbances from seismic waves of earthquakes.

A persistent increase in the permeability of rock mass due to transient stress disturbances could also explain the increase in petroleum production caused by earthquakes or artificial vibrations (Beresnev and Johnson, 1994; Pride et al., 2008), as observed in enhanced oil recovery (Beresnev et al., 2005). Manga et al. (2012) also noted the possibility that seismic waves induce earthquakes in the intermediate and far fields. Even the decrease in giant ($M \geq 8$) earthquakes between the 1960s and the 1990s when the United States, the Union of Soviet Socialist Republics, and other countries frequently carried out underground nuclear explosion tests (Fujii et al., 2017; Fujii et al., 2018b) could be explained by the induction of numerous small earthquakes that occurred as a result of variations in rock mass permeability due to transient stress disturbances from the seismic waves of the test explosions.

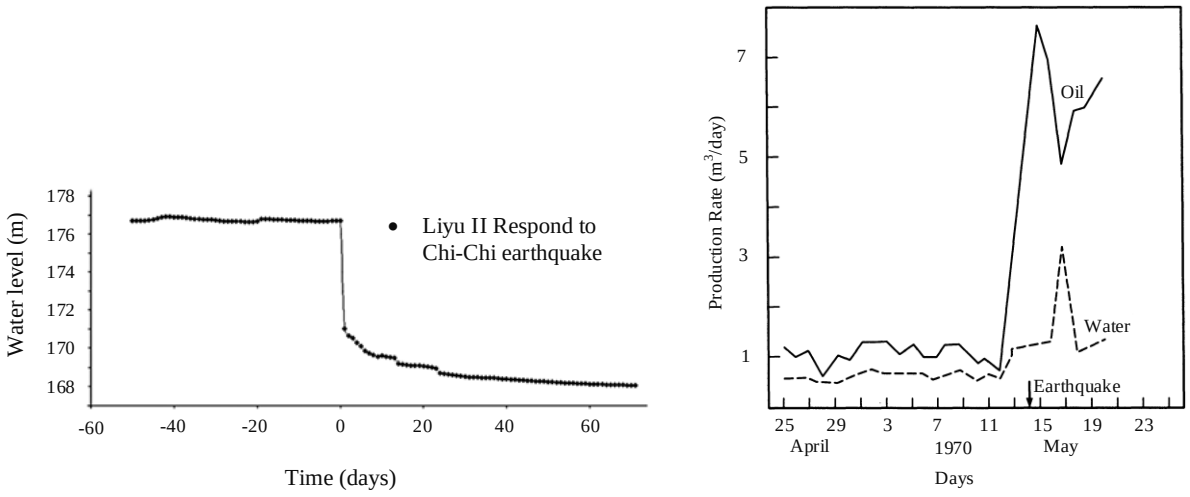

(a) (b)

Fig. 1.1 Example of phenomena related to earthquakes. (a) Water level of Liyu II well decreased due to M_W 7.5 Chi-Chi earthquake in Taiwan in 1999; the well was located about 5 km from the surface rupture of the causative faults (Wang & Chai, 2008), and (b) the step-like increase in oil and water productions due to M_W 6.5 earthquake in Daghestan in 1970; the wells were located about 50 km from the epicenter (Beresnev & Johnson, 1994).

1.2 Statement of the problem and objectives of the study

To clarify the effects of transient stress disturbances, several laboratory and in-situ tests have been carried out (Table 1). Tests on Berea sandstone demonstrated increase in the permeability of intact rock (Roberts, 2005) and fractured in situ rock under pore pressure disturbances (Elkhoury et al., 2011). In another experiment conducted on three types of rock (limestone, basalt and gabbro), axial stress disturbances induced an increase and a decrease in the permeability at high (130–250 °C) and low (20 °C) temperatures, respectively (Shmonov et al., 1999). Liu & Manga (2009) showed that the permeability of fractured sandstone decreased due to axial stress disturbances.

It is recognized from the results of the above laboratory tests that the effects of transient stress disturbances on rock permeability have not been clarified yet and data accumulation for different types of rock under various conditions is necessary. Furthermore, it is difficult to compare the results from previous studies (Table 1) because the rock types were different from study to study, the permeability was measured for only one rock condition (intact, fractured or in situ), and for only one type of

disturbances (pore pressure, axial displacement or axial stress) in each study. The permeability values of both the intact and fractured rock specimens were therefore measured for Kushiro Cretaceous sandstone and Shikotsu welded tuff, and the disturbance types included both transient axial stress and pore pressure so that the effects of transient stress disturbances on the permeability between rock types, rock conditions and disturbance types could be compared and analyzed in this study. The experiment was then rather focused to the effects of the multiple transient axial stress disturbances on permeability of triaxially fractured Inada granite.

Table 1.1 The experimental conditions and the effect of stress disturbances on the permeability

Experiments	Frequency (Hz)	Peak amplitude	Disturbances	Samples		Permeability response
Elkhoury et al. (2011)	0.05	0.02–0.3 MPa	Pore pressure	Fractured in *situ*	Berea sandstone	Increase
Roberts (2003)	25–27	0.3–1.2 MPa	Axial stress	Intact	Berea sandstone	Increase
Shmonov et al. (1999)	0.05–20	10^{-4}–10^{-3}	Axial strain	Intact	Limestone, basalts, gabbro	Increase (high T=130°C–250°C) Decrease (Low T=20°C)
Liu & Manga (2009)	0.3–2.5	10^{-4}	Axial strain	Fractured	Sandstone	Decrease

1.3 Outline of the research

The dissertation is divided into 6 chapters as follows:

Chapter 1 includes the research background, statement of the problem and objectives of the study, and the structure of the dissertation. Chapters 2, 3 and 4 cover the experiments on Kushiro Cretaceous

sandstone, Shikotsu welded tuff and Inada granite, respectively. Rock sample, experimental methodology, test results and discussions on each rock are presented in each chapter. In Chapter 5, the effects of transient stress disturbances on the rocks are discussed. Chapter 6 provides the overall conclusions, the possible application of the transient stress disturbances and suggestion for future research.

2. Experiment on
Kushiro Cretaceous sandstone

		Page No.
2.1	Rock samples	7-8
2.2	Sample preparation and experimental setup	8-9
2.3	Experimental procedure and condition	9-12
2.4	Results and discussions	12-18
	2.4.1 Transient disturbances in axial stress	12
	2.4.2 Transient disturbances in pore pressure	16

2.1 Rock sample

The Kushiro Cretaceous sandstone was sampled from the borehole No. 72, in the depth of 322.65 to 323.50 m, from the second drilling pit at the inclined shaft 650 m from the entrance (Fig. 2.1) of Kushiro Coal Mine (Fujii et al., 2011), which is located in the eastern region of Hokkaido, Japan. Methane gas has been extracted from the Cretaceous layer underlying the Paleogene coal bearing formation.

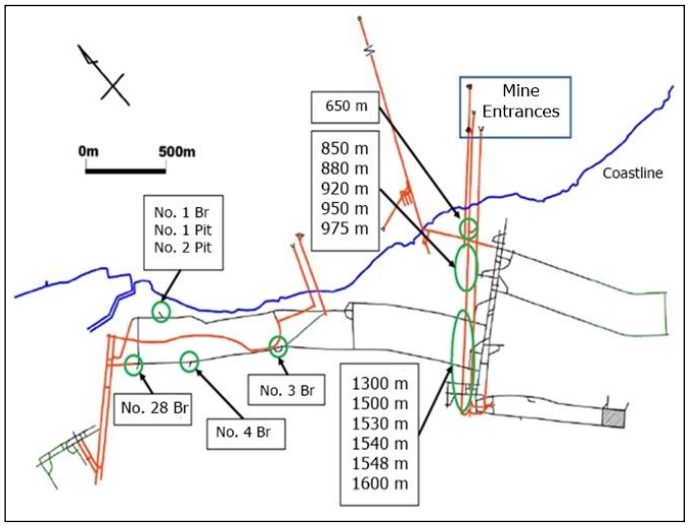

Fig. 2.1 Location of gas wells for Cretaceous rock mass at Kushiro Coal Mine (Matsumoto et al., 2014).

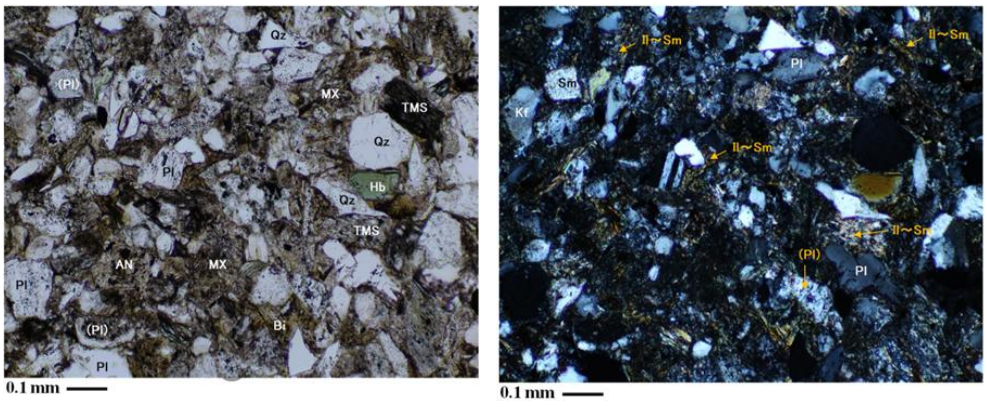

(a) Open Nicol (b) Crossed Nicols

Fig. 2.2 Microscopic images of the Kushiro Cretaceous sandstone. Qz: quartz ($\phi \leq$ 0.2–0.4 mm), Pl: plagioclases ($\phi \leq$ 0.2 mm), Mx: matrix (Sm~Il: smectite ~ illite (silt-size mineral pieces)), Kf: potash feldspar ($\phi \leq$ 0.2 mm), Bi: biotite:$\phi \leq$ 0.2–0.5 mm), Hb: ordinary amphibole ($\phi \leq$ 0.15 mm), AN: andesite ($\phi \leq$ 0.2 mm), TMS: transformed mudstone ($\phi \leq$ 0.25 mm)), Mc: mica, Chl: chlorite).

The rock mainly consists of a matrix of quartz, plagioclases and silt-size smectite (Fig. 2.2, Table 2.1) and is classified as a wacke fine-grained sandstone. The grain sizes of the quartz are between 0.2–0.4 mm and the plagioclase grains are less than 0.2 mm and have an angular to subangular form. The amount of organic carbon was about 0.15 to 0.59% and the C/N ratio was in the range of 7.0 to 14.0 (Matsumoto et al., 2014). The average porosity is 11% (Table 2.2).

Table 2.1 Mineral composition of the Kushiro Cretaceous sandstone from XRD analysis. Qz: Quartz, Pl: Plagioclases, Kf: Potash feldspar, Am: Amphibole, Hm: Hematite, Mc: Mica, Chl: Chlorite, Sm: Smectite

Qz	Pl	Kf	Am	Hm	Mc	Chl	Sm
Very abundant	Very abundant	Abundant	Very little	Little	Little	Little	Medium

Table 2.2 Physical properties of the rock samples shown as the average value (number of specimens) ± standard deviation

Properties	Kushiro Cretaceous sandstone	
	Dry	Saturated
Porosity (%)	10.53 (9) ± 2.43	
Density (g/cm^3)	2.37 (9) ± 0.02	2.48 (9) ± 0.02
V_P (km/s)	3.35 (9) ± 0.14	3.04 (9) ± 0.16

2.2 Sample preparation and experimental setup

Cylindrical specimens (30 mm diameter, 60 mm high) were bored from the 65 mm diameter cores along the vertical drilling axis (Fig. 2.3). The specimens were dried at 80°C in an oven for approximately two days before being vacuum saturated in pure water. Each specimen was connected to a pair of stainless steel end-pieces that had a center hole to allow water to flow through the specimen. A coating of silicon sealant was applied to the lateral surface of each specimen to maintain the water flow within the specimens. A heat-shrinkable tube was used to jacket the specimen with end-pieces to prevent direct contact of the confining fluid with the specimen. Each jacketed specimen

was vacuum saturated again for 24 hours and placed in the ultracompact triaxial cell (Alam et al., 2014; Fig. 2.4).

(a) (b)

Fig. 2.3 (a) Cores of Kushiro Cretaceous sandstone and (b) Specimen coring.

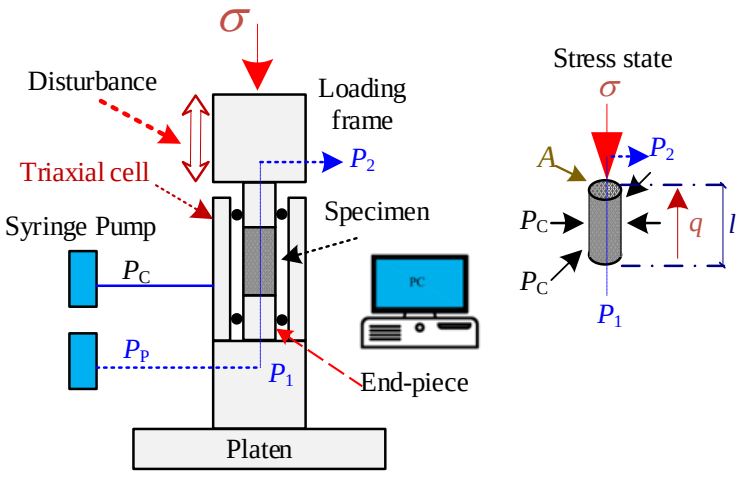

Fig. 2.4 The permeability measurement apparatus.

2.3 Experimental procedure and conditions

The confining pressure was set up 3, 10 or 15 MPa (Table 2.3). The pore pressure of 1 MPa was applied at the bottom of the specimen, and the upper end of the specimen was open to the atmosphere (Fig. 2.4). The axial stress disturbances were triangular at 0.5 Hz for 200 s (Fig. 2.5a) and the amplitude was up to 11 MPa. The rectangular disturbances of pore pressure were between 0.2 and 1.8 MPa. The disturbances had a duration of approximately 200 s, with frequency between 0.05 to 0.18 Hz under a 10 MPa confining pressure (Table 2.3 and Fig. 2.5b). Considering the low permeability, a 10^{-5}

s^{-1} (0.036 mm/s) strain-rate controlled triaxial compression was applied. It should be noted that the axial stress disturbances for the intact rocks might also have caused pore pressure disturbances inside the specimens because of the low permeability. On the contrary, pore pressure disturbances would not have induced axial stress disturbances even for intact specimens because the response of the loading frame was sufficiently rapid.

The disturbance frequency was first set at 0.5 Hz for the axial stress disturbances on the Kushiro Cretaceous sandstone simulating a moderate earthquake. However, the frequency was adjusted because of the limiting speed for the manual operation of the syringe pump and it was finally set at 0.05 Hz. The results would have been slightly affected by the differences in the disturbance wave shapes. Further, the differences in the disturbance frequency may have quantitatively affected the results. However, the effects of this difference would not be sufficient to lead to opposite conclusions.

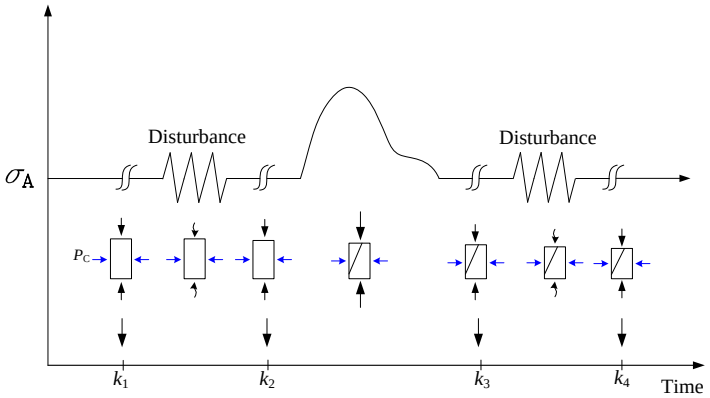

(a) Axial stress disturbances

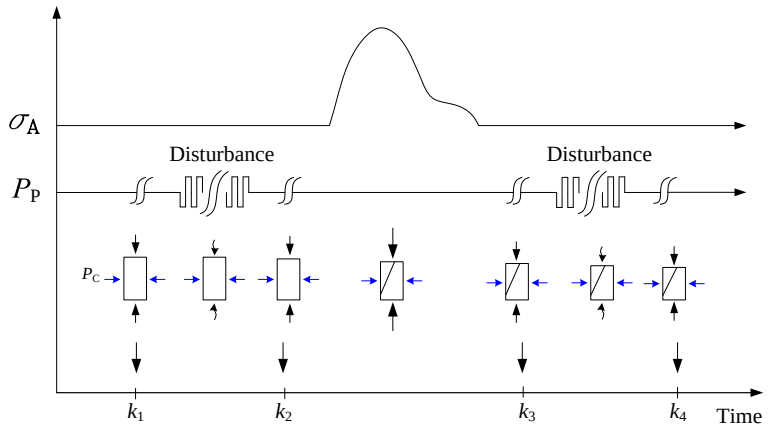

(b) Pore pressure disturbances

Fig. 2.5 Experimental procedure.

Table 2.3 Experimental conditions for the Kushiro Cretaceous sandstone (P_C: confining pressure, P_P: pore pressure, $\Delta\sigma_A$: axial stress disturbance amplitude, ΔP_P: pore pressure disturbance amplitude, P_P-min: minimum pore pressure, P_P-max: maximum pore pressure, f: frequency)

Axial stress disturbances			
Samples	P_C (MPa)	$\Delta\sigma_A$ (MPa)	f (Hz)
AS-KCS1	3	1	0.5
AS-KCS2	10	0	
AS-KCS3		1	
AS-KCS4		3	
AS-KCS5		4	
AS-KCS6		5	
AS-KCS7		7	
AS-KCS8		9	
AS-KCS9		11	
AS-KCS10	15	1	
AS-KCS11		5	

Pore pressure disturbances					
Samples	ΔP_P (MPa)	P_P-min (MPa)	P_P-max (MPa)	f (Hz)	P_C (MPa)
P_P-KCS1	0.2	0.9	1.1	0.15	10
P_P-KCS2	0.6	0.7	1.3	0.09	
P_P-KCS3	0.8	0.9	1.7	0.05	
P_P-KCS4	1	0.5	1.5	0.18	
P_P-KCS5	1.4	0.3	1.7	0.09	
P_P-KCS6	1.8	0.1	1.9	0.1	
P_P-KCS7	1.8	0.1	1.9	0.1	
P_P-KCS8	1.86	0.07	1.93	0.12	
P_P-KCS9	1.88	0.07	1.95	0.1	

The water level of the syringe pump was recorded at 1 min interval. The permeability values of the intact rock before and after the transient stress disturbances in the prefailure regime, k_1 and k_2, respectively, and those of the fractured rock before and after the transient stress disturbances in the postfailure regime, k_3 and k_4, respectively, were evaluated by substituting the average flow rate over 24 hours into the following Darcy's equation:

$$k = \frac{q\mu}{A}\left(\frac{\mathrm{d}p}{\mathrm{d}x}\right)^{-1} \tag{2.1}$$

where k (m^2) is the permeability, q is the flow rate (m^3/s), μ is the fluid viscosity (Pa·s), A is the cross-sectional area (m^2) of the specimen, and dp/dx is the pressure gradient (Pa/m). The viscosity of water (μ) is 9.57×10^{-4} (Pa·s) at 295 K, which is the air temperature of the testing room that was kept constant with the aid of an air conditioner. The flow rate for Fig. 2.7 and 2.13 was evaluated for every 1 hour for detail observation.

2.4 Results and discussions

2.4.1 Transient disturbances in axial stress

All Kushiro Cretaceous sandstone samples showed brittle failure (Fig. 2.6a). The maximum stress under the 10 MPa confining pressure was in the range of 90–150 MPa and slightly increased as the transient stress amplitude increased (Fig. 2.6b).

Examples of the variation in permeability, and the impacts of transient stress disturbances and failure for the average permeability are shown in Figs. 2.7 and 2.8, respectively. The permeability of this sandstone increased by the failure (observed in the variation in permeability in Hold-2 to Hold-3 in Fig. 2.7, or k_2 to k_3 in Fig. 2.8) as was reported for Kimachi sandstone, which is a Neogene tuffaceous sandstone in Japan (Alam et al., 2014).

The permeability of the intact specimen, which is basically shown in Hold-1 and Hold-2, was reduced, even with no stress disturbances (Fig. 2.9a), and the reduction was not affected by the axial stress disturbance amplitude (Fig. 2.7 and Fig. 2.9a). However, the reduction increased as the

confining pressure increased (Fig. 2.9b). According to the above results, the permeability reduction of the intact rock (decrease in permeability from Hold-1 to Hold-2, or k_1 to k_2, Fig. 2.9) could mainly be attributed to consolidation over time under the confining pressure.

The decreased effect on permeability was observed for fractured rocks referring to Hold-3 (pre-disturbance) and Hold-4 (post-disturbance) (Fig. 2.7). The reduction from k_3 to k_4 of the fractured rocks was small at zero stress disturbance amplitude, and it increased with the disturbance amplitude (Fig. 2.10a). This decrease in permeability did not depend on the confining pressure (Fig. 2.10b). Therefore, the above described usual consolidation would not be a predominant mechanism. Instead, the stress disturbances may have been enhanced either by the closure of the rupture planes or by the production of fine gouge particles (Fig. 2.11c) with the sizes varying from 10 μm to 500 μm. They either caused clogging or settling at the points of the rupture planes with the smallest apertures (Fig. 2.11d, Bear, 1979; Wang & Manga 2009; Elkhoury et al., 2011).

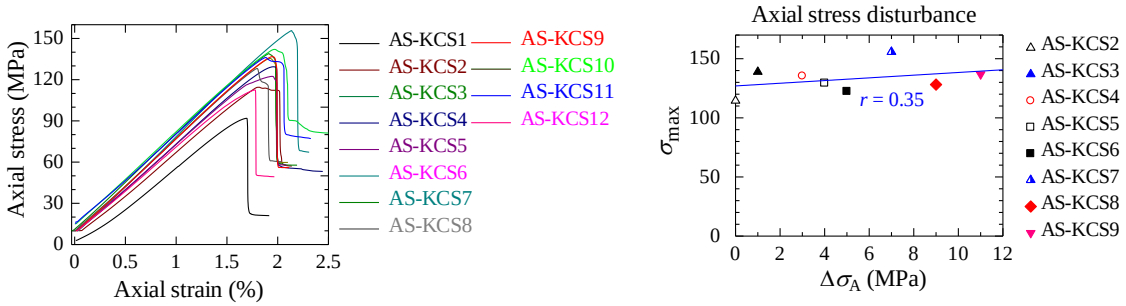

(a) (b)

Fig. 2.6 (a) Stress–strain curves and (b) maximum stress (σ_{max}) vs. the amplitudes of the axial stress disturbances ($\Delta\sigma_A$) under P_C = 10 MPa of the Kushiro Cretaceous sandstone.

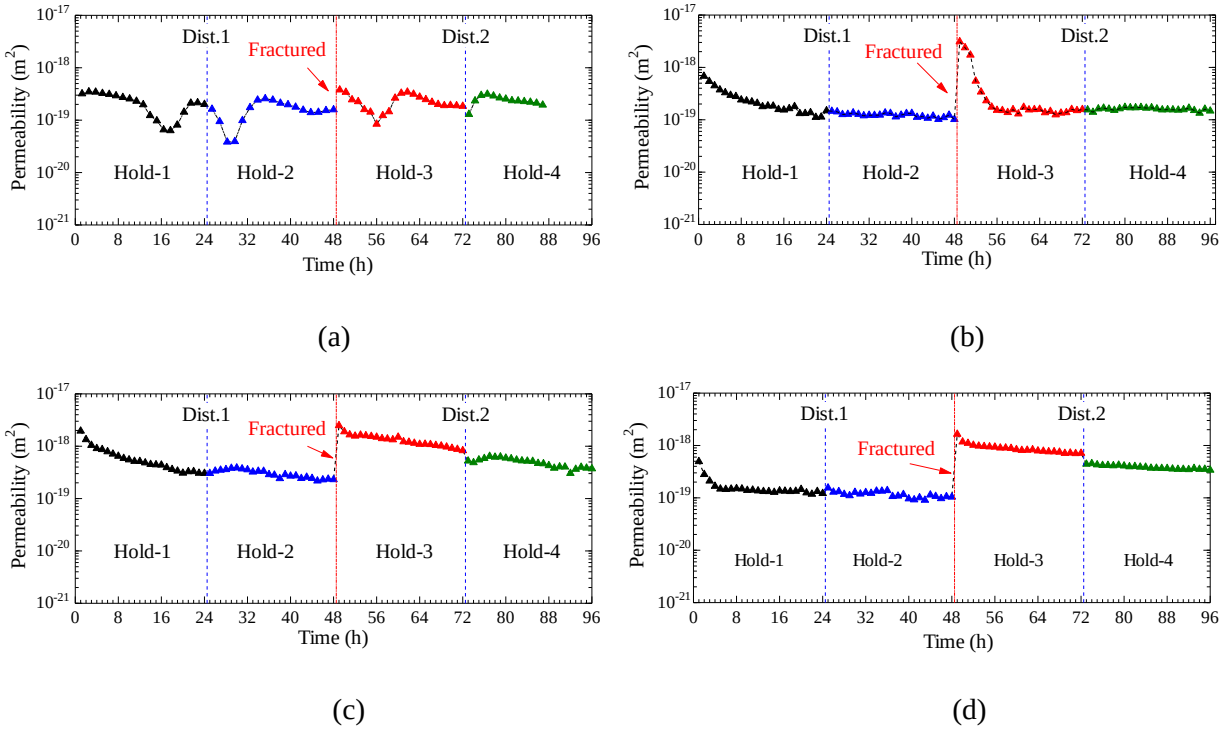

Fig. 2.7 Variation in permeability in each hydrostatic stress state (Hold-1, Hold-2, Hold-3, and Hold-4) at the time of axial stress disturbance for the entire experiment: (a) AS-KCS2, (b) AS-KCS5, (c) AS-KCS8, and (d) AS-KCS9. Dist. 1 and Dist. 2 are the disturbances in prefailure and postfailure.

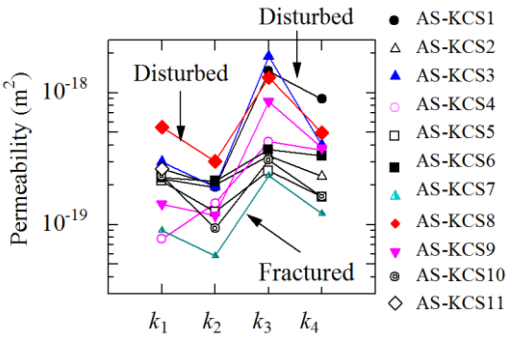

Fig. 2.8 Variation in permeability in each hydrostatic stress state at the time of axial stress disturbances and triaxial compression.

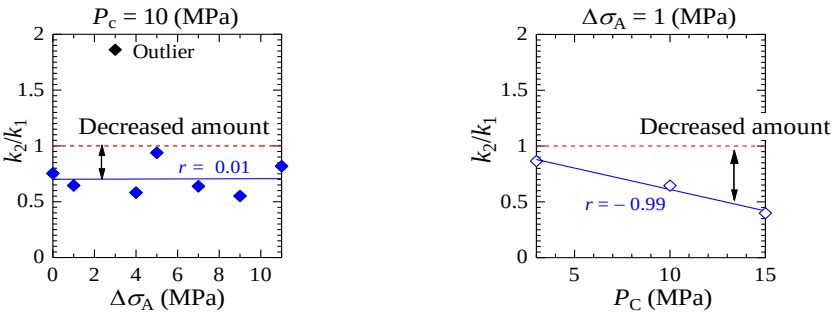

(a) (b)

Fig. 2.9 Permeability ratio vs. (a) axial stress disturbance amplitude and (b) confining pressure of the intact rocks. The outlier data point was ignored for the regression analysis.

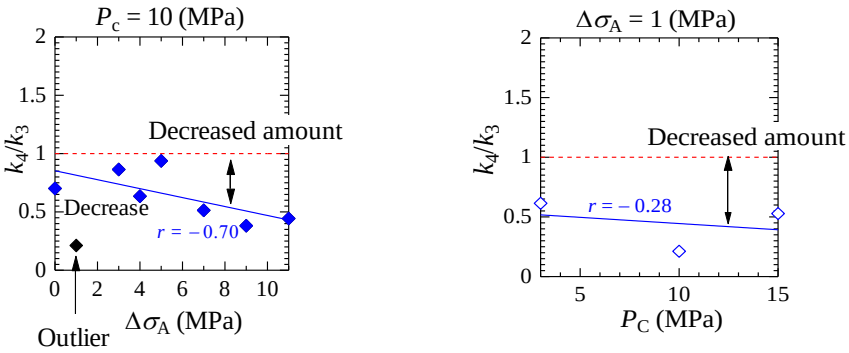

(a) (b)

Fig. 2.10 Permeability ratio vs. (a) axial stress disturbance amplitude and (b) confining pressure of the fractured rocks.

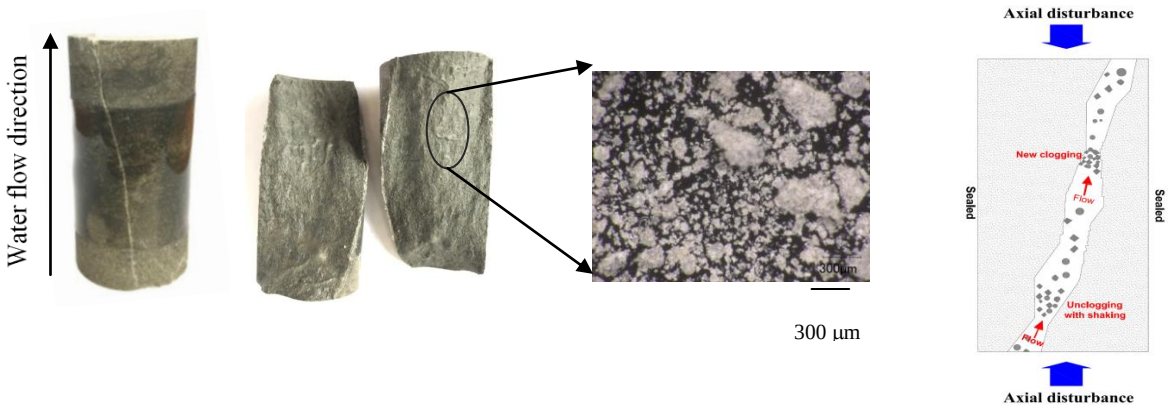

(a) (b) (c) (d)

Fig. 2.11 A specimen after an experiment (Pp-KCS3): (a) specimen showing the rupture plane, (b) gouge along the rupture plane, (c) microscopic image of the particles along the rupture plane, and (d) clogging and unclogging of an aperture by particles (Liu & Manga, 2009).

2.4.2 Transient disturbances in pore pressure

Specimens for the pore pressure disturbance tests were prepared from another rock core obtained from a slightly different depth. All specimens failed in a brittle manner (Fig. 2.12a). The maximum stresses were in the range of 70–90 MPa and increased slightly with the pore pressure disturbance amplitude (Fig. 2.12b).

Permeability increased due to failure (k_2 to k_3) but decreased due to pore pressure disturbances (k_1 to k_2, and k_3 to k_4) (Figs. 2.13 and 2.14). The *y*-intercept of Fig. 2.15a shows the reduction in the intact rock permeability (k_1 to k_2) at zero disturbances. This would imply the effect of consolidation over time. The reduction decreased as the pore pressure disturbance amplitudes increased. Even for a specimen, k_2 was larger than k_1 under larger pore pressure disturbances (Figs. 2.13c and 2.15a). This increase in the permeability could be induced by the formation of microfractures due to the pore pressure disturbances. However, as shown in Fig. 2.12b, the strength was not reduced with pore pressure disturbances, and hence, the formation of microfractures would not be the main mechanism. The removal of the barriers that clogged the existing pathways (Bai & Tien, 1997; Manga et al., 2012; Beresnev et al., 2011) would be a preferable explanation for this finding.

The reduction in permeability due to pore pressure disturbances for the fractured specimens (in postfailure, Hold-3 to Hold-4 in Fig. 2.13, or k_3 to k_4 in Fig. 2.15b) was not very large at zero disturbances and slightly increased as the pore pressure disturbance amplitude increased, although the *r* value (the coefficient of correlation) is low. The mechanisms would be similar to those of the fractured rocks with axial stress disturbances.

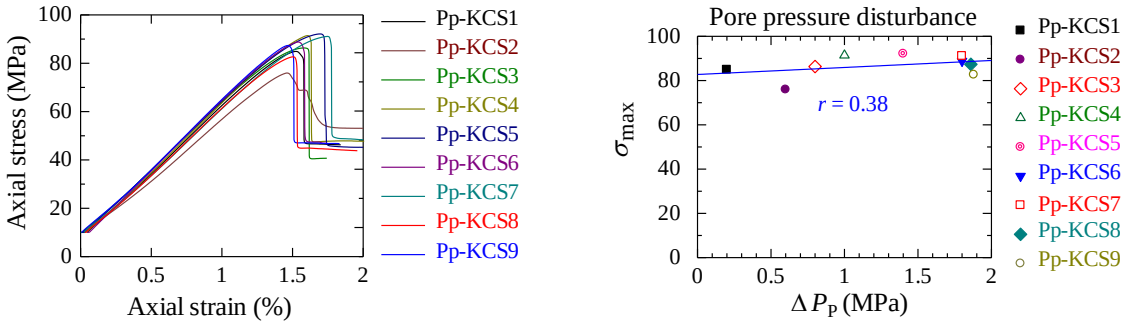

(a) (b)

Fig. 2.12 (a) Stress–strain curves and (b) maximum stress (σ_{max}) vs. amplitudes of the pore pressure disturbances (ΔP_P) of the Kushiro Cretaceous sandstone.

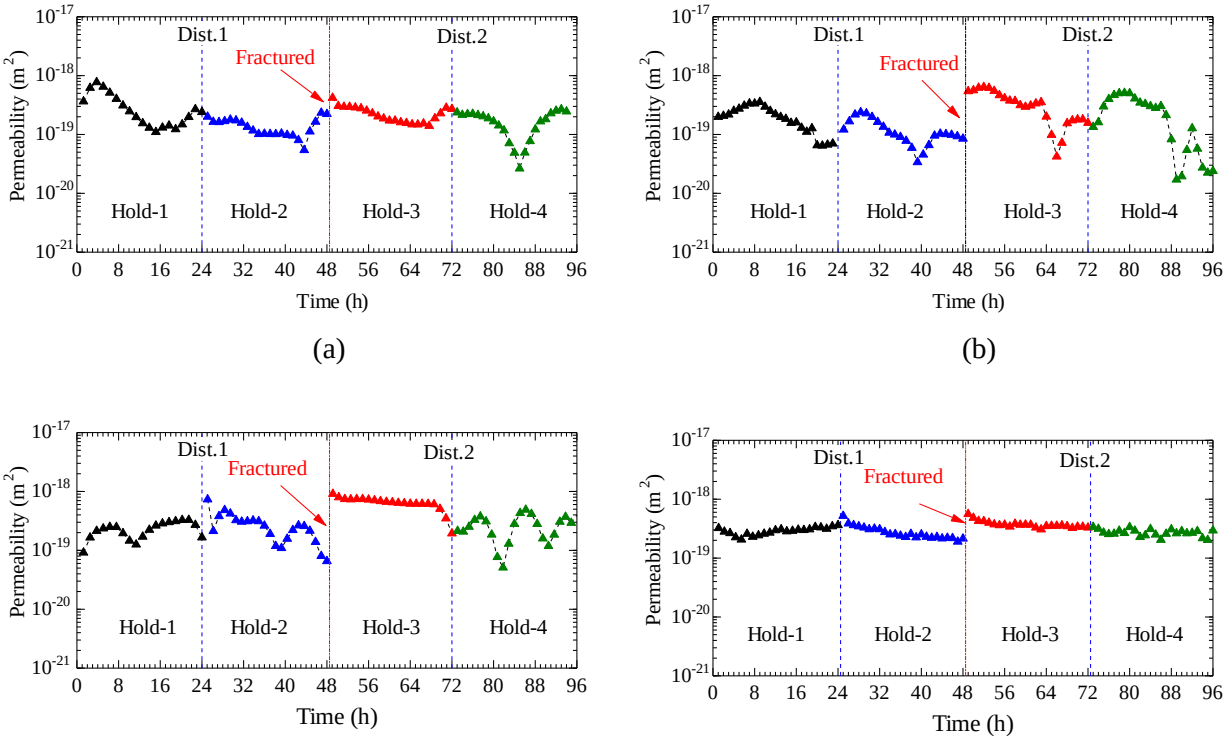

Fig. 2.13 Variation in permeability in each hydrostatic stress state (Hold-1, Hold-2, Hold-3, and Hold-4) at the time of transient pore stress disturbances for the whole experiment: (a) P_P-KCS1, (b) P_P-KCS4, (c) P_P-KCS6, and (d) P_P-KCS7. Dist. 1 and Dist. 2 are the disturbances in prefailure and postfailure, respectively.

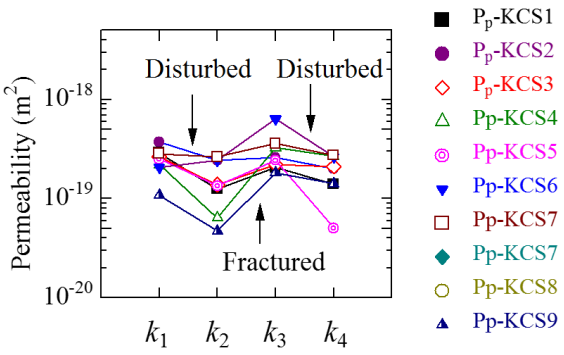

Fig. 2.14 Permeability variation due to pore pressure disturbances and triaxial compression under P_C = 10 MPa.

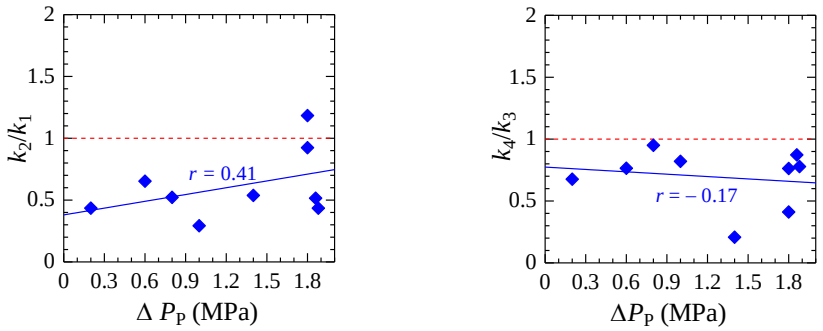

(a) (b)

Fig. 2.15 Effect of pore pressure disturbances on the permeability ratio of the Kushiro Cretaceous sandstone, (a) intact rocks and (b) fractured rocks.

3. Experiment on
Shikotsu welded tuff

		Page No.
3.1	Rock sample	20-20
3.2	Sample preparation and experimental setup	20-21
3.3	Experimental procedure and condition	21-23
3.4	Results and discussions	23-28
	3.4.1 Transient disturbances in axial stress	24
	3.4.2 Transient disturbances in pore pressure	26

3.1 Rock sample

A rock block of Shikotsu welded tuff having the porosity of 32% (Table 3.1) was taken from Sapporo, Japan. The glassy rock sample, which originated from pyroclastic deposits from the eruption of the Shikotsu volcano 40,000 years ago, is predominantly composed of plagioclase, hypersthene, augite, hornblende, and transparent volcanic glass having a felt-like structure in the matrix (Fig. 3.1). The mineral grain sizes are between 0.3–1.5 mm for the plagioclase, approximately 0.5 mm for the hypersthene, 0.3–0.7 mm for the augite, and 0.5–1.0 mm for the hornblende (Doi, 1963).

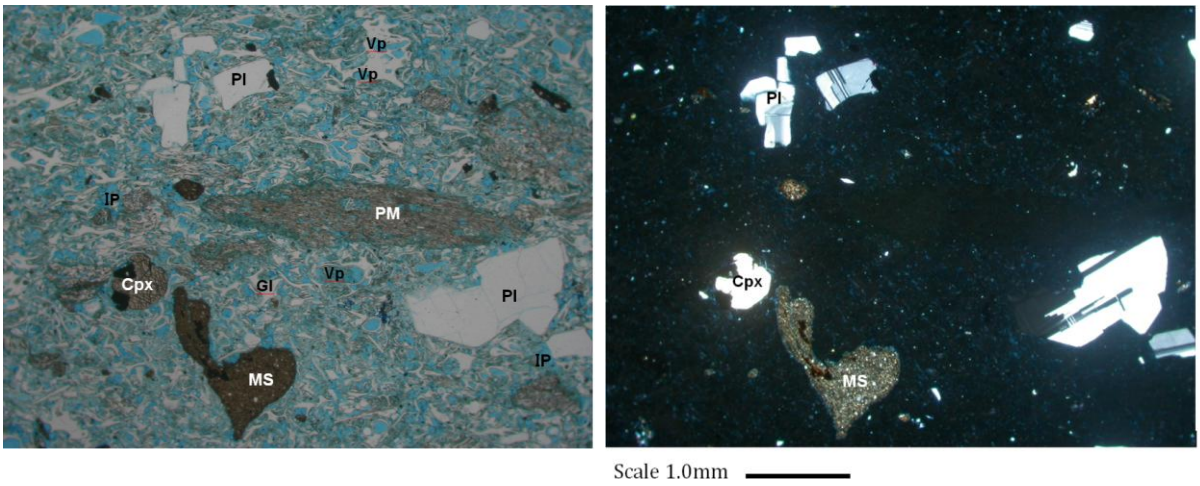

(a) Open Nicol (b) Crossed Nicols

Fig. 3.1 Microscopic images of the Shikotsu welded tuff. Pl: plagioclase, Hb: amphibole, Cpx: clinopyroxene, IP: intergranular pore, PM: pumice, Gl: glass, MS: mudstone, Vp: vesiculated pore.

Table 3.1 Physical properties of the rock samples shown as the average value (number of specimens) ± standard deviation

Properties	Shikotsu welded tuff	
	Dry	Saturated
Porosity (%)	31.65 (18) ± 1.65	
Density (g/cm^3)	1.30 (18) ± 0.01	1.62 (18) ± 0.02
V_P (km/s)	2.14 (18) ± 0.07	1.92 (18) ± 0.14

3.2 Sample preparation and experimental setup

P-wave velocity was measured along each pair of opposite sides of the rock block of Shikotsu welded tuff with 140-kHz sensors (Fig. 3.2). Cylindrical specimens (30 mm diameter and 60 mm long) were bored from the rock block along the slowest (1.67 km/s) P-wave velocity direction. The velocities in the two other perpendicular directions were 1.82 km/s and 2.11 km/s. The specimen preparation and the experimental setup are similar to those for Kushiro Cretaceous sandstone.

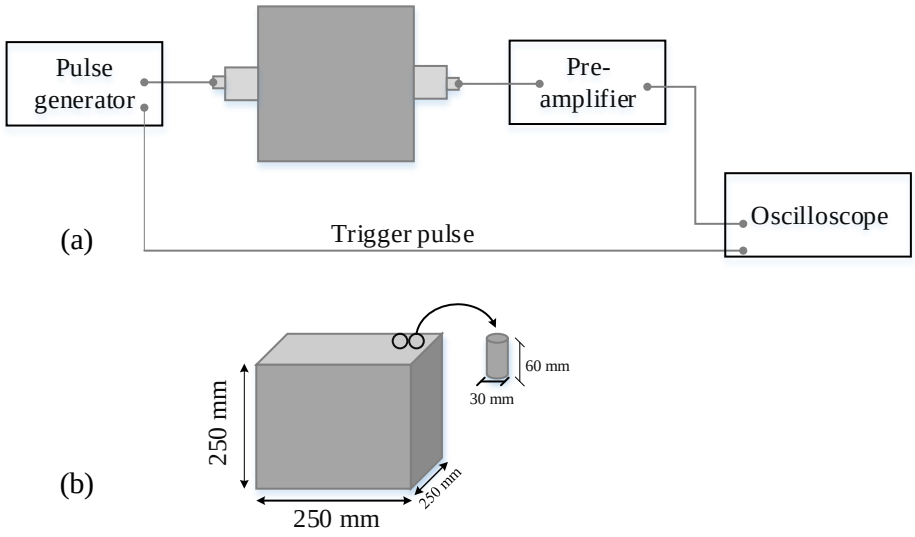

Fig. 3.2 Specimen from the Shikotsu welded tuff block. (a) Measuring P-wave velocity of the block (b) coring direction and core specimen.

3.3 Experimental procedure and conditions

Nearly rectangular axial stress disturbances were applied with pore pressure of 0.1 and 0.5 MPa and a confining pressure of 5 MPa (Fig. 3.3a). Axial stress disturbance amplitudes of 0 or 8 MPa at 0.05 Hz for 200 seconds were applied (Table 3.2). The same pore pressure, confining pressure and disturbance frequency were used for the rectangular transient pore pressure disturbances. The applied disturbance amplitudes were between 0 and 0.8 MPa. The triaxial compression rate was set at 10^{-4} s^{-1} (0.36 mm/s), considering the high permeability. The axial stress disturbances would not cause pore pressure disturbances inside a specimen even for the intact rocks because of their high permeability.

Permeability was calculated in the similar way to Kushiro Cretaceous sandstone except that the holding time was 60 s and the sampling interval of water volume was 1s (Fig. 3.3).

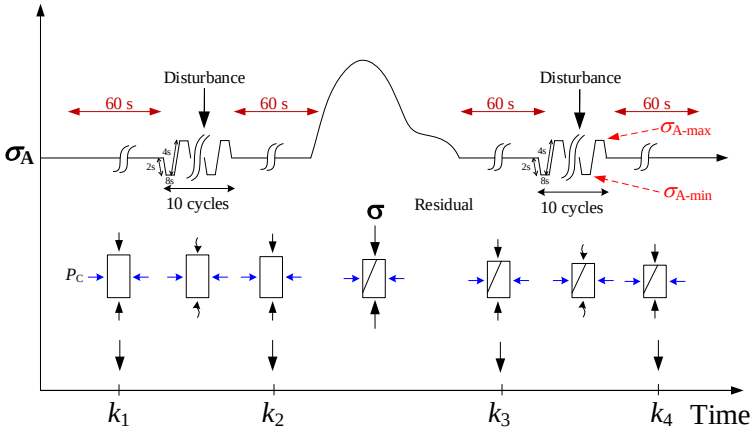

(a) Axial stress disturbances

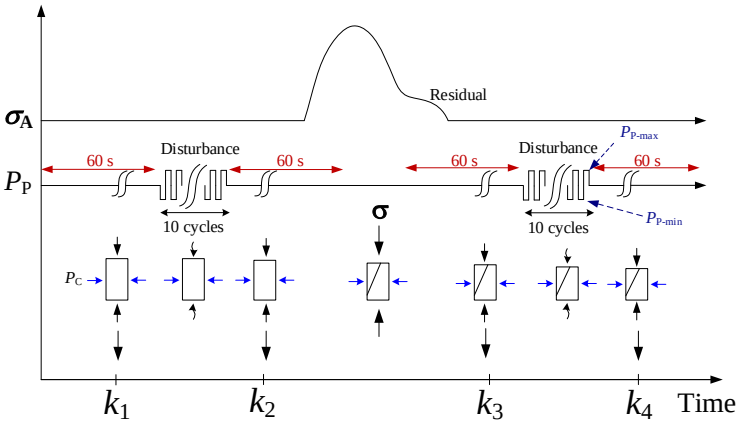

(b) Pore pressure disturbances

Fig. 3.3 Experimental procedure for the Shikotsu welded tuff.

Table 3.2 Experimental condition for the Shikotsu welded tuff (P_C: confining pressure, P_P: pore pressure, $\Delta\sigma_A$: axial stress disturbance amplitude, ΔP_P: pore pressure disturbance amplitude, P_P-min: minimum pore pressure, P_P-max: maximum pore pressure)

Axial stress disturbances				Pore pressure disturbances					
Samples	$\Delta\sigma_A$ (MPa)	P_P (MPa)	P_C (MPa)	Samples	ΔP_P (MPa)	P_P-min (MPa)	P_P-max (MPa)	P_P (MPa)	P_C (MPa)
AS-T1	0	0.5	5	Pp-T1	0	0.5	0.5	0.5	5
AS-T2				Pp-T2					
AS-T3				Pp-T3					
AS-T4	8			Pp-T4	0.1	0.45	0.55		
AS-T5				Pp-T5					
AS-T6				Pp-T6					
AS-T7	0	0.1		Pp-T7	0.8	0.1	0.9		
AS-T8				Pp-T8					
AS-T9				Pp-T9					
AS-T10	8			Pp-T10	0	0.1	0.1	0.1	
AS-T11				Pp-T11					
				Pp-T12					
				Pp-T13	0.06	0.07	0.13		
				Pp-T14					
				Pp-T15					

3.4 Results and discussions

The Shikotsu welded tuff specimens failed in a ductile manner with slight stress drops (Figs. 3.3a and 3.4a). The maximum stress was affected by neither the axial stress (Fig. 3.3b) nor the pore pressure disturbances (Fig. 3.4b).

3.4.1 Transient disturbances in axial stress

The axial stress disturbance tests were conducted under 0.5 (Fig. 3.6) or 0.1 MPa (Fig. 3.7) pore pressure. With the application of 0.5 MPa pore pressure, the permeability showed an increase for the intact rocks (Fig. 3.6b). This would have occured because of the cleaning of the pore throats and the micropathways by the rapid water flow (Bai & Tien, 1997; Bergendahl & Grasso, 2000; Liu & Manga, 2009). The increased permeability was not affected by the disturbance amplitude (Fig. 3.6b). The permeability decreased from k_2 to k_3 due to rock failure (Fig. 3.6a), and this result is the same as those presented by Alam et al. (2014) for the same rock type. This reduction in permeability may be due to the crushing of the matrix that consists of volcanic glass (Fig. 3.10a). The permeability further decreased from k_3 to k_4 at zero disturbances (Fig. 3.6c). This would be due to the closure of the rupture planes and the clogging of the smallest apertures by some fine particles over time. These decreases were reduced as the disturbance amplitude increased (Fig. 3.6c). This would be due to the generation and unclogging of the microfracture paths (Fig. 3.10b) (Elkhoury et al., 2006; Liu and Manga, 2009; Elkhoury et al., 2010; Manga et al., 2012).

Under a pore pressure of 0.1 MPa, the permeability decreased from k_1 to k_2 and k_3 (Fig. 3.7a). The reduced permeability from k_1 to k_2 (Fig. 3.7b) was almost constant with the axial stress disturbance amplitudes for the intact rocks. This may suggest that the rock was slightly consolidated over time and that the water flow was not sufficiently rapid to clean up the pore throats. The permeability decreased for the fractured rocks at zero stress disturbances (k_3 to k_4, Fig. 3.7c). However, the reduction decreased as the stress disturbances increased (Fig. 3.7c), which was probably due to mechanisms similar to those of the 0.5 MPa case (Fig. 3.6c).

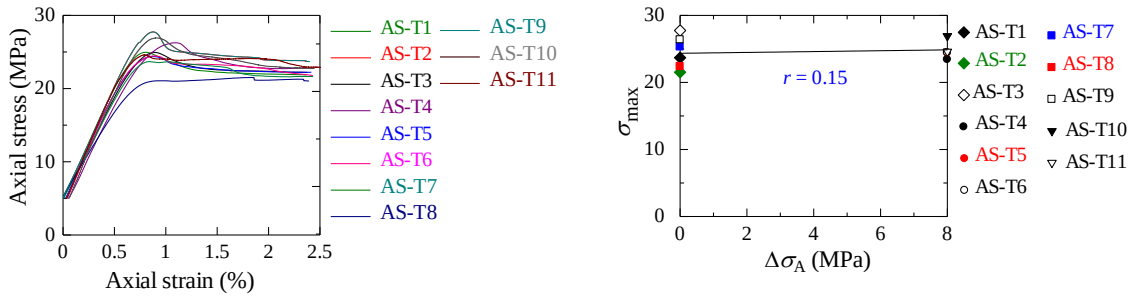

(a) (b)

Fig. 3.4 (a) Stress–strain curves and (b) maximum stress (σ_{max}) vs. amplitude of the axial stress disturbaned ($\Delta\sigma_A$) Shikotsu welded tuff.

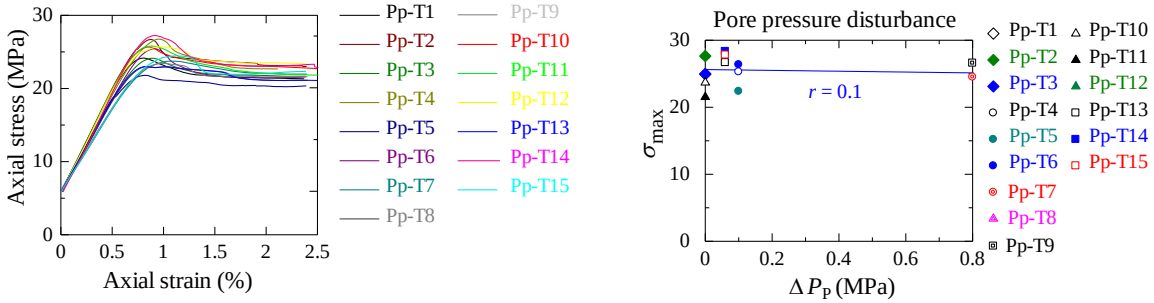

(a) (b)

Fig. 3.5 (a) Stress–strain curves and (b) maximum stress (σ_{max}) vs. the amplitude of the pore pressure disturbance (ΔP_P) Shikotsu welded tuff.

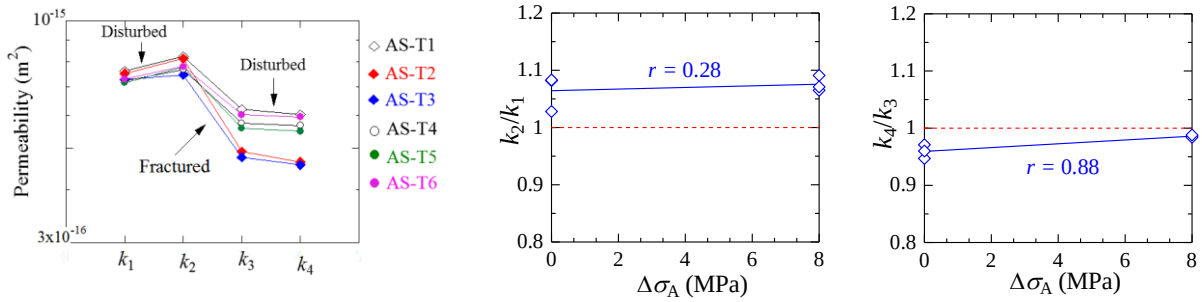

(a) (b) (c)

Fig. 3.6 (a) Variation in permeability, and permeability ratios of the intact rocks (b) and fractured rocks (c) (P_P = 0.5 MPa) due to transient axial stress disturbances and triaxial compression of the Shikotsu welded tuff.

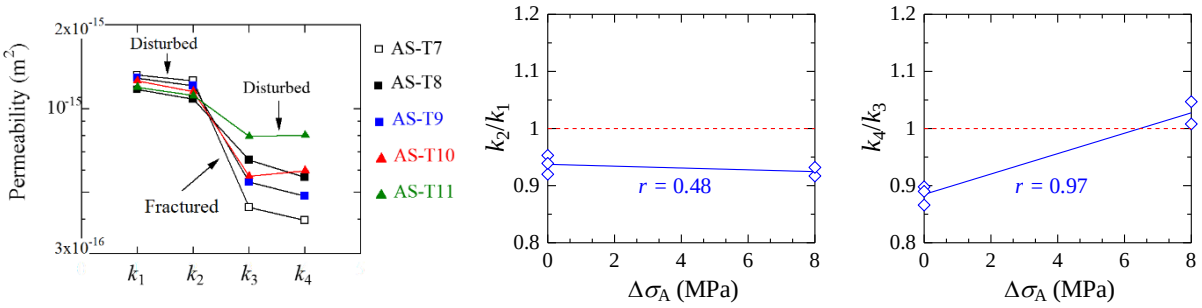

(a) (b) (c)

Fig. 3.7 (a) Variation in permeability, and permeability ratios of the intact rocks (b) and fractured rocks (c) (P_P = 0.1 MPa) due to transient axial stress disturbances and the triaxial compression of the Shikotsu welded tuff.

3.4.2 Transient disturbances in pore pressure

The pore pressure disturbances that were performed under 0.5 MPa in pore pressure (Fig. 3.8) exhibited results that were similar to those of the axial stress disturbance.

The results under 0.1 MPa in pore pressure (Fig. 3.9) were also similar to those of the axial stress disturbances. However, the effects of the disturbances were not clear because the amplitude of the pore pressure disturbances at 0.1 MPa pore pressure was just 0.06 MPa. The results basically showed a good repeatability of the tests, except for the reduction of the permeability due to rock failure, which varied from specimen to specimen.

The k_2/k_1 ratio with zero disturbances was found to be less than one at 0.1 MPa in pore pressure and greater than one at 0.5 MPa in pore pressure (Fig. 3.11a). This is the same result that was found for the axial stress disturbances and would indicate that, for the intact rocks, a higher pore pressure promoted a more rapid flow that cleaned up the trapped particles in the pore throats (Brodsky et al., 2003; Roberts, 2005; Candela et al., 2014; Candela et al., 2015). Fractured rocks experienced a greater reduction in permeability under the lower pore pressure (Fig. 3.11b), which may suggest that more particles were accumulated owing to the slower water flow.

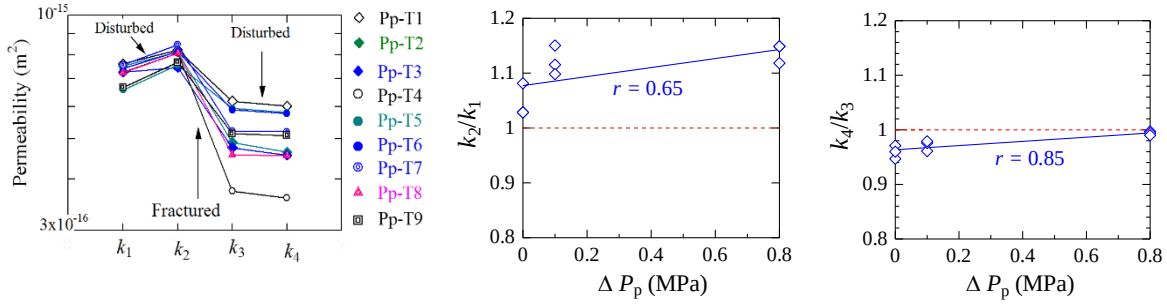

(a) (b) (c)

Fig. 3.8 (a) Variation in permeability and permeability ratios of the intact rocks (b) or fractured rocks (c) (P_P = 0.5 MPa) due to transient pore pressure disturbances and triaxial compression of the Shikotsu welded tuff.

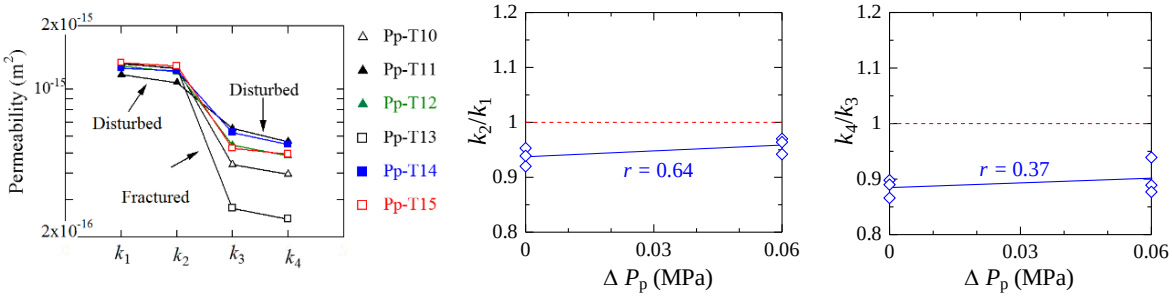

(a) (b) (c)

Fig. 3.9 (a) Variation in permeability and permeability ratios of the intact rocks (b) and the fractured rocks (c) due to transient pore pressure disturbances and triaxial compression of the Shikotsu welded tuff (P_P = 0.1 MPa).

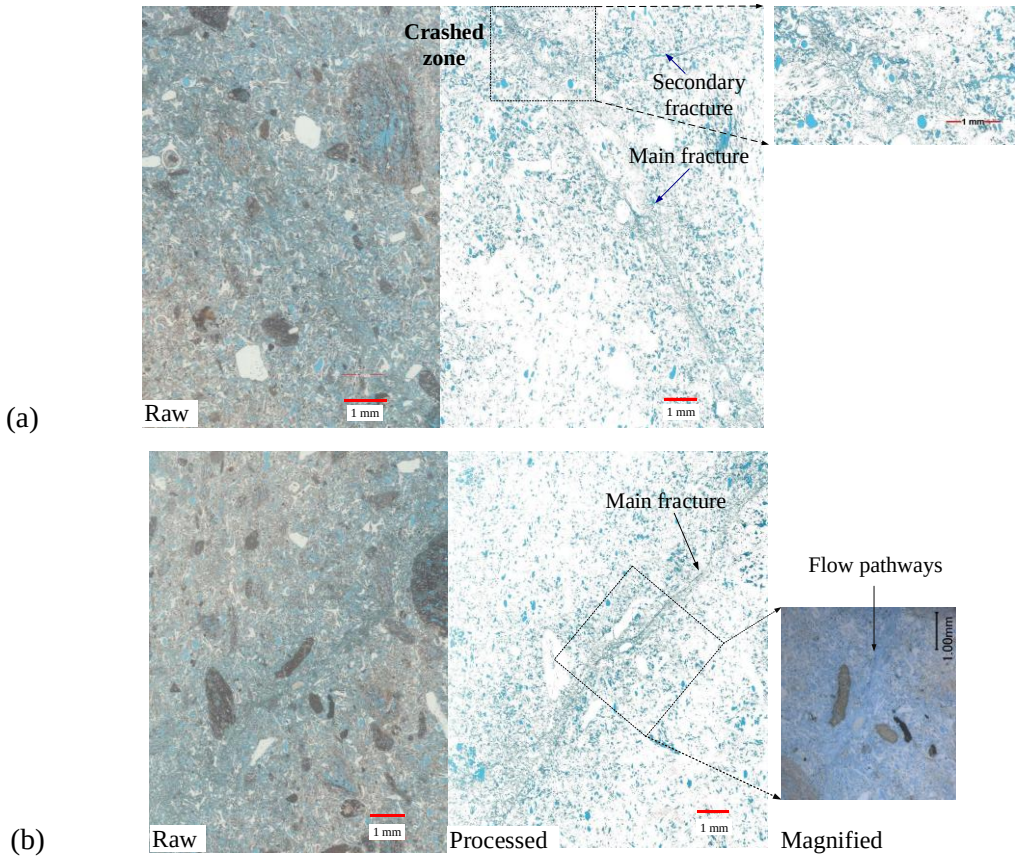

Fig. 3.10 Images of blue resin impregnated thin-section samples after the tests under (a) $\Delta\sigma_A$ = 8 MPa, P_C = 5 MPa, P_P = 0.5 MPa, and (b) ΔP_P = 0.8 MPa, P_C = 5 MPa, P_P = 0.5 MPa. Left: original images, middle: processed images to emphasize the blue resin, and right: magnified images.

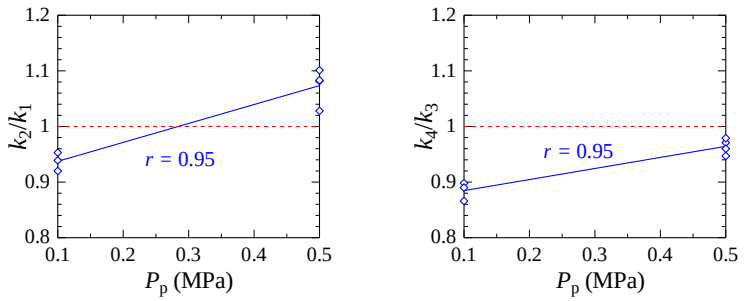

(a) Intact (b) Fractured

Fig. 3.11 Effect of pore pressure on permeability ratios without stress disturbances.

4. Experiment on
Inada granite

		Page No.
4.1	Rock samples	30-30
4.2	Sample preparation and experimental setup	30-31
4.3	Experimental procedure and conditions	31-32
4.4	Results	32-38
4.5	Discussions	38-39

4.1 Rock sample

A 250 mm cubic block of Inada granite from Kasama, Japan was used. The 60 Ma granite is mainly composed of coarse to medium grains of quartz, plagioclase, alkali-feldspar and biotite (Fig. 4.1) (Oda et al., 2002) with the average grain size in a range of 1–4 mm (Table 4.1) (Lin & Takahashi, 2008). The porosity is 0.35 ± 0.07% from the dry and wet densities of 2.512 ± 0.037 g/cm^3 and 2.517 ± 0.039 g/cm^3, respectively for seven specimens.

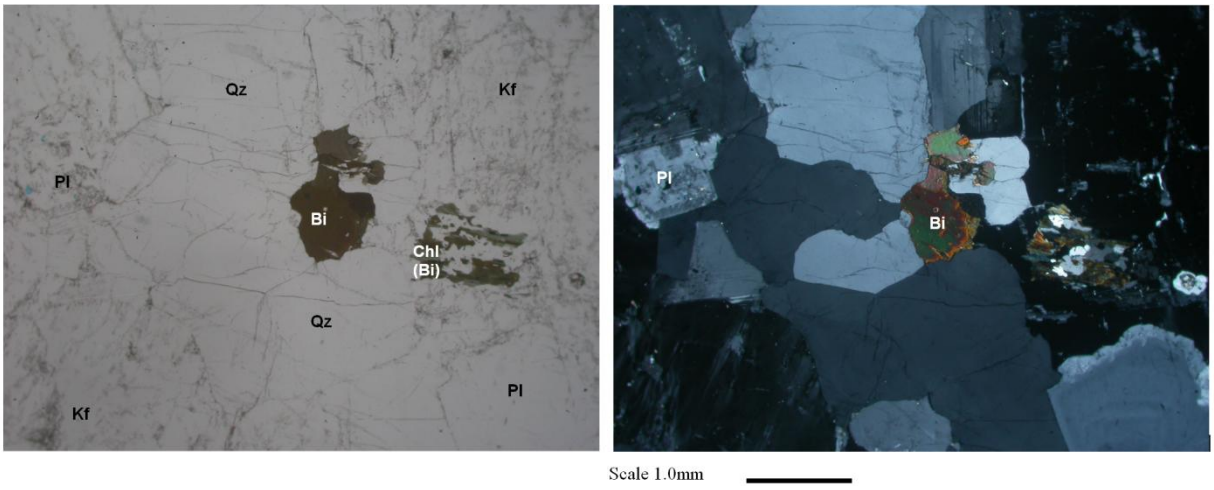

(a) open Nicol (b) Crossed Nicols

Fig. 4.1 Microscopic images of Inada granite. Qz: Quartz, Pl: plagioclase, Kf: potash feldspar, Bi: biotite.

Table 4.1 Mineral composition and grain sizes of Inada granite (Lin & Takahashi, 2008)

Mineral	Amount (%)	Average grain sizes (mm)	Maximum grain size (mm)
Quartz	36	3 – 4	4
Plagioclase	32	2 – 3	4
Alkali-feldspar	28	2 – 4	5
Biotite	4	1	3

4.2 Sample preparation and experimental setup

Cylindrical specimens with a diameter and length of 30 mm and 60 mm, respectively were drilled

along the axis with the lowest V_P (4.16 km/s) of the rock block. The velocities in the two other perpendicular directions were 4.44 km/s and 4.23 km/s. The specimens were then dried at 80°C in an oven for approximately 3 days before being vacuum saturated in pure water for 4 days. The experimental setup was the same as the previous rocks.

4.3 Experimental procedure and conditions

A confining pressure of 5 MPa was set using a syringe pump, and pore pressure of 1 MPa was applied at the bottom of the specimen using another syringe pump. The upper end of the specimen was open to atmospheric pressure (Fig. 2.4). The specimen was then triaxially fractured at a constant strain rate of 10^{-5}/s (or 0.036 mm/min) until the residual strength state was achieved. The fractured specimen was kept under constant hydrostatic pressure for 60 min (Hold-1), then transient disturbances in the axial stress were applied at 0.05 Hz for 200 s (Dist. 1, Fig. 4.1); the steps were performed iteratively for Hold–2, Dist. 2, Hold–3, Dist. 3, and Hold–4. The load and stroke were recorded for every 1 μm variation in the stroke.

The water volume in the syringe pump for pore pressure was recorded at 1 Hz during the disturbances and the flow rate was calculated from the regression line of the water volume for 3 s moving window for Fig. 4.3. The water volume was recorded every minute during the Hold steps and the flow rate was calculated from the regression line for every 3 data points for Fig. 4.5. The permeability was calculated by substituting the flow rate into Equation 2.1.

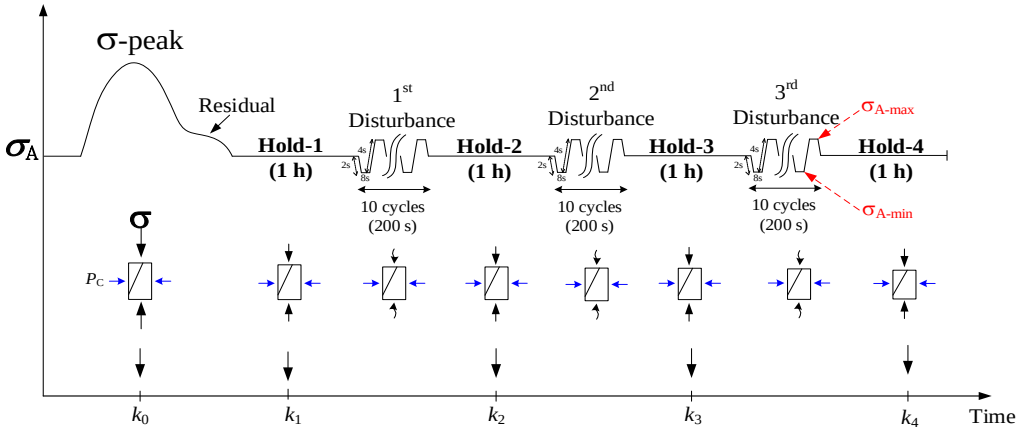

Fig. 4.2 Experimental procedure.

Table 4.2 Experimental conditions under multi axial stress disturbances

Sample	Transient stress disturbances	
	$\Delta\sigma_A$ (MPa)	Peak values (MPa)
IG-1	0	5.0–5.0
IG-2	1	4.5–5.5
IG-3	3	3.5–6.5
IG-4	5	2.5–7.5
IG-5	5	2.5–7.5
IG-6	8	1.0–9.0
IG-7	8	1.0–9.0

4.4 Results

All the samples showed brittle failure (Fig. 4.3). The peak stress and the residual strength were in the range of 220–260 MPa and 30–40 MPa, respectively. Pore water flowed into the specimen when the axial stress decreased and flowed back to the syringe pump when the axial stress increased during the disturbances (Fig. 4.4). The axial strain decreased during Hold-1 and slightly increased during Hold-2 to Hold-4 (Fig. 4.5). The result shows apparent decrease in the axial strain with each series of disturbances.

The permeability was highest at the beginning of Hold−1 because of fracturing, but decreased with time (Fig. 4.6). The disturbance amplitudes did not affect the ratio of the permeability at the end of the test to that at the beginning, k'_4/k_1 (Fig. 4.7) as indicated by the low correlation coefficient (Fig. 4.8a). However, the permeability increased with each series of axial stress disturbances for amplitudes of 3 MPa or larger (Figs. 4.6c–g). The permeability ratios of each series of disturbances, k_2/k'_1, k_3/k'_2, and k_4/k'_3 (Fig. 4.7) roughly increased with the disturbance amplitudes (Fig. 4.8b). The permeability (k_n) decreased with time and recovered to its value before the disturbances (k'_{n-1}) during each Hold step. The time of the recovery Δt (Fig. 4.7) for amplitudes of 5 MPa and 8 MPa was larger than that at smaller amplitudes (Fig. 4.8c).

A major single fracture was observed under zero axial stress disturbances (Fig. 4.9a). Intergranular microcracks as well as multiple fractures were observed under axial stress disturbances (Figs. 4.9b–g). The size of the gouge between the rupture planes was analyzed by sieving using mesh sizes of 500 μm, 150 μm, 75 μm, and 53 μm (Figs. 4.10a and 4.10b). The amount of gouge increased with the axial stress disturbance amplitudes (Fig. 4.10c). The ratio of the ultrasonic velocity of the fractured specimen to that of the intact specimen decreased with the axial stress disturbance amplitudes (Fig. 4.11). The reduction in ultrasonic velocity suggests more fracturing by axial stress disturbances (Saroglou & Kallimogiannis, 2017; Xing et al., 2018).

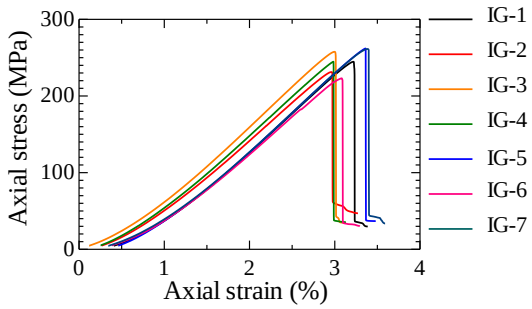

Fig. 4.3 Stress–strain curves.

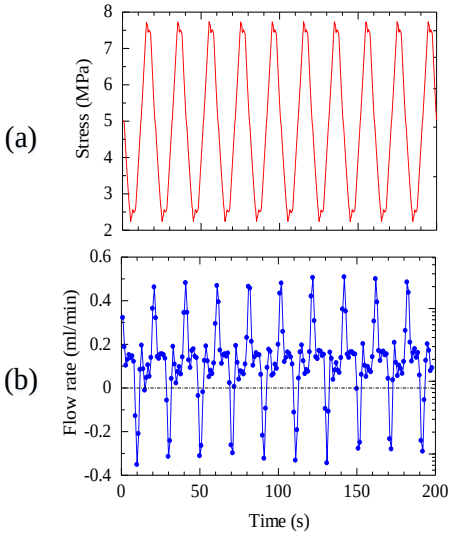

Fig. 4.4 Variations in (a) axial stress and (b) water flow rate with time (IG-4, moving average of Dist.1 for 3 s).

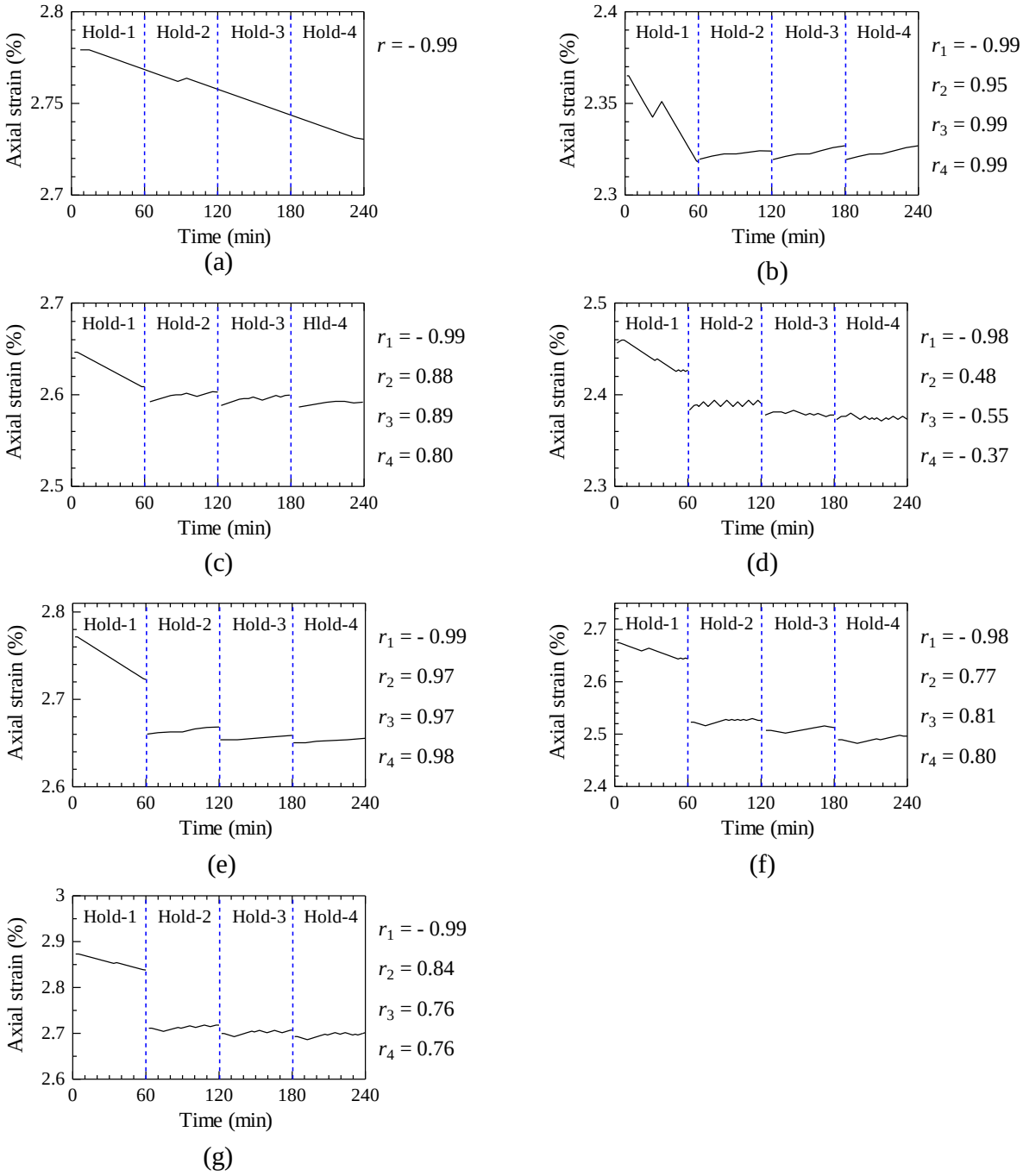

Fig. 4.5 Variations in axial strain during Hold-1–4: (a) IG-1, (b) IG-2, (c) IG-3, (d) IG-4, (e) IG-5, (f) IG-6, and (g) IG-7.

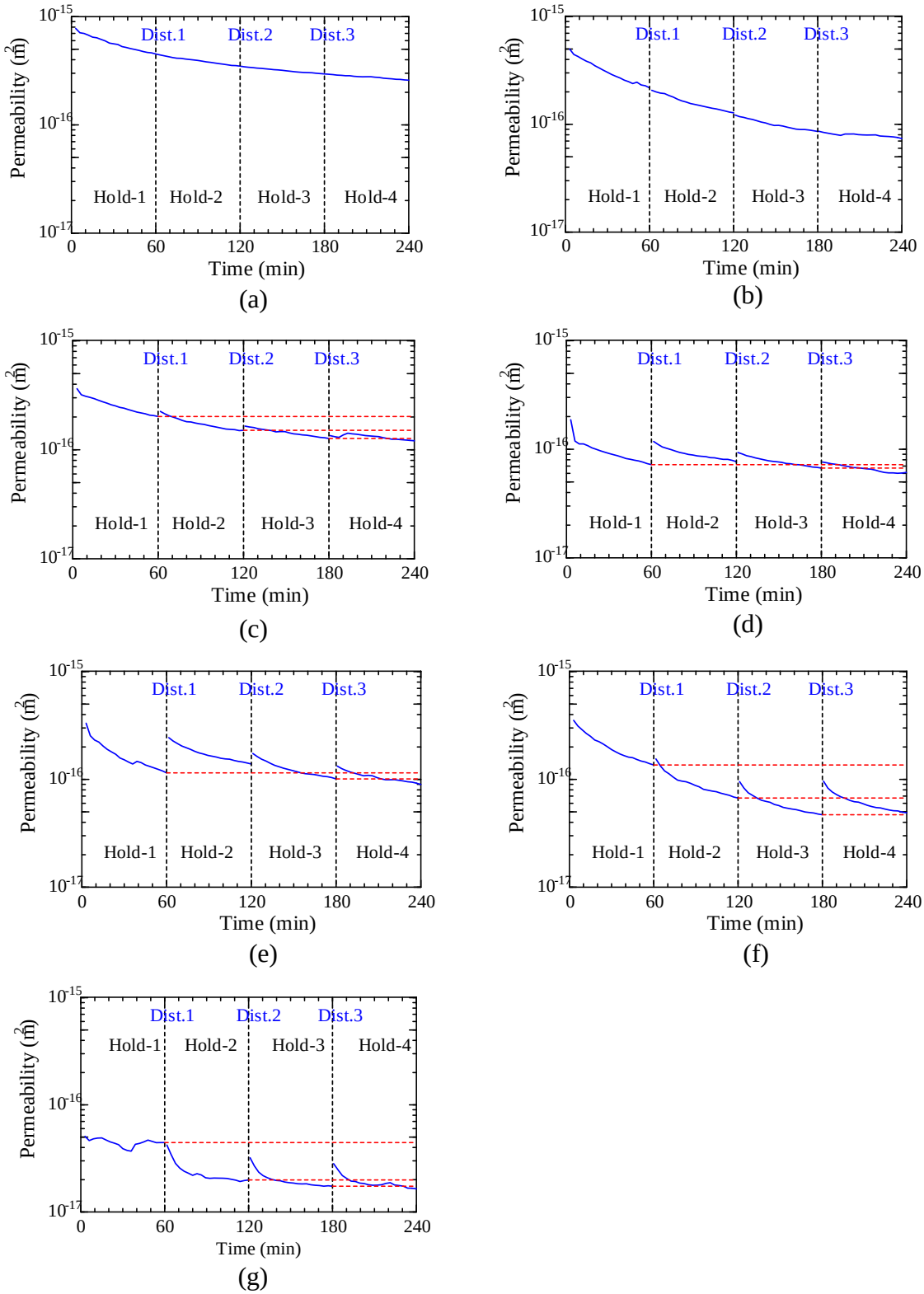

Fig. 4.6 Variations in permeability due to multiple transient axial stress disturbances: (a) IG-1, (b) IG-2, (c) IG-3, (d) IG-4, (e) IG-5, (g) IG-6, and (f) IG-7.

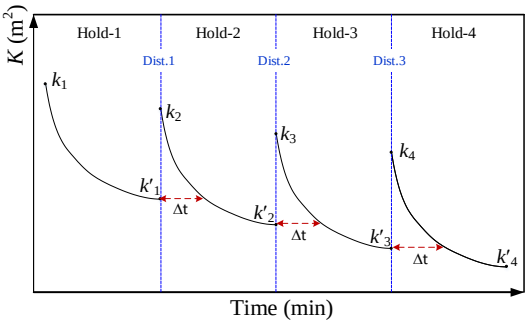

Fig. 4.7 Definition of k_n, k'_n, and Δt.

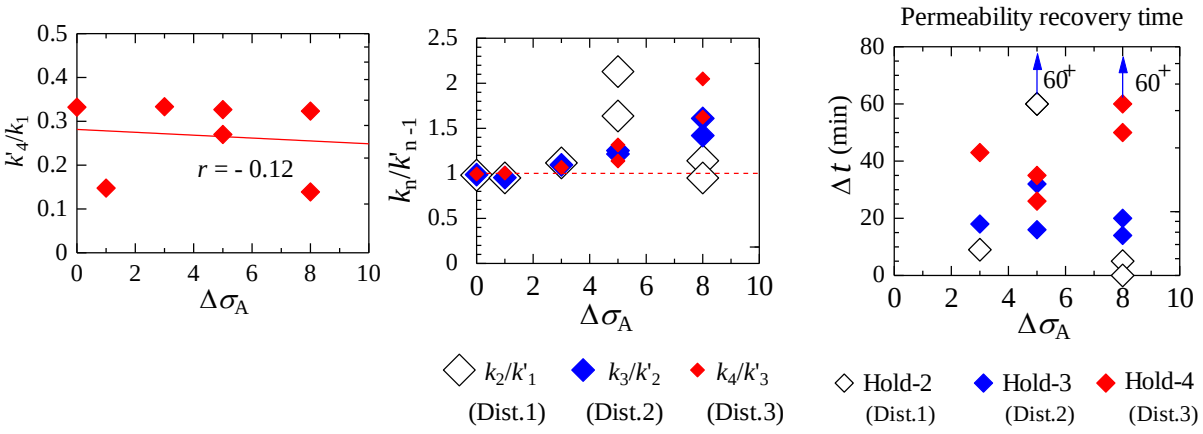

(a) (b) (c)

Fig. 4.8 Effects of axial stress disturbance amplitudes on (a) permeability ratio k'_4/k_1, (b) ratio of permeability after axial stress disturbances (k_n) to that before the disturbances (k'_n), and (c) time of decrease to the level before the disturbances (k_n to k'_{n-1}).

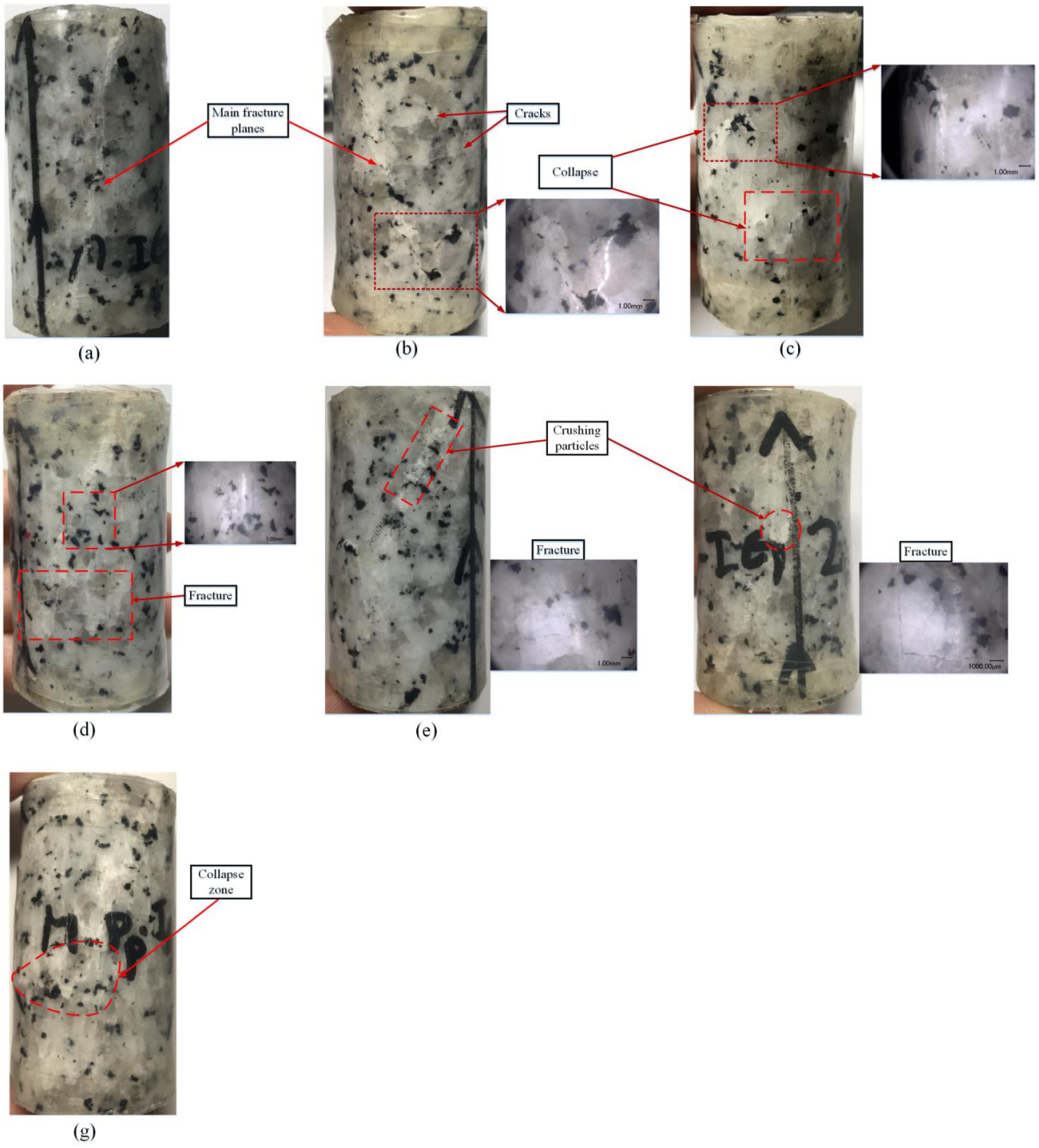

Fig. 4.9 Specimens after the experiment: (a) IG-1, (b) IG-2, (c) IG-3, (d) IG-4, (e) IG-5, (f) IG-6, and (g) IG-7.

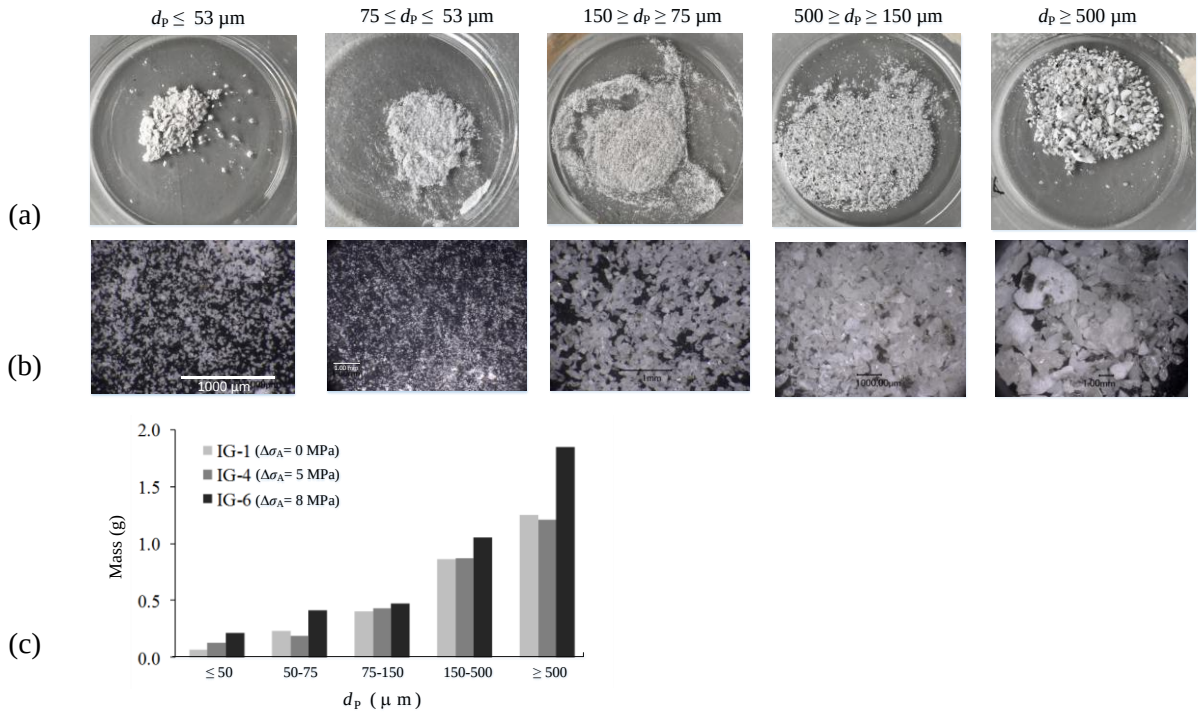

Fig. 4.10 (a) Gouge between the rupture planes after sieving (IG-4). (b) Gouge under microscope (IG-4). (c) Particle size distribution of gouge for IG-1, IG-4, and IG-6.

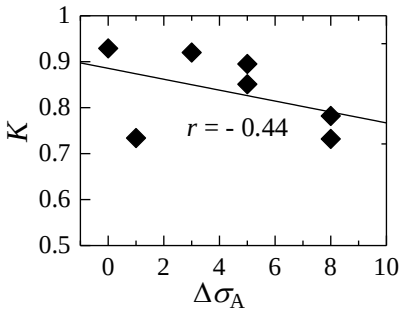

Fig. 4.11 Ratio of ultrasonic velocity of tested specimens to that before the test, *K*.

4.5 Discussions

The decrease in the axial strain with time in Hold-1 (Fig. 4.5) would be due to the anelastic strain recovery (Matsuki & Takeuchi, 1993; Lin et al., 2006) with decrease in stress from the residual strength to the hydrostatic pressure. The slight increase in axial strain during each step of Hold-2 to Hold-4 (Fig. 4.5) may be due to creep deformation.

The degree of reduction in the permeability at the end of the test was not affected by the axial stress disturbance amplitudes (Fig. 4.8a). The reduction in the permeability with time (Fig. 4.6) is therefore mainly due to the time-dependent closure of the rupture plane as a result of anelastic strain recovery under hydrostatic pressure.

The axial stress disturbances induced persistent increase in permeability (Figs. 4.6 and 4.8). The decrease in the axial strain (Fig. 4.5) due to the disturbances suggests that the persistent increase in permeability is mainly due to the increase in the aperture of the rupture plane as a result of slip which was propped by the hard fines. The removal of fine particles from the flow pathways due to fluctuation in water flow (Fig. 4.4b) is also one of the mechanisms of the increase in permeability. The flow rate enhanced increase in permeability was stated in Candela et al. (2015) by mobilization of the fines. The increase of fractures with the axial stress disturbances by the direct observation (Fig. 4.9) and V_P measurement (Fig. 4.11) may have also contributed to the persistent increase in permeability.

The permeability decreased with time and recovered to its initial value before the disturbances (Fig. 4.6). This would be mainly as a result of viscous deformation of the rupture plane. Permeability recovery is also as a result of clogging of water flow pathways by fine particles (Lui & Manga, 2009; Wang et al., 2016; Boeut et al., 2019). The time of permeability recovery was in the order of several tens of minutes. This may be too short for field applications. However, if the time is proportional to the size of the affected rock mass, then the time for a rock mass of several tens of meters, for example, would be in the order of one week, which is sufficient for certain applications.

5. Effects of transient stress disturbances on permeability

The permeability of the Kushiro Cretaceous sandstone (Table 5.1) decreased at zero stress disturbances. For the intact rocks, the permeability reduction became larger as the confining pressure increased, but this was not exhibited by the fractured rocks. In terms of the axial stress disturbance effects, the permeability was kept almost constant with the disturbance amplitude for the intact rocks. The reductions became larger as the disturbance amplitudes increased for the fractured rocks. Regarding the pore pressure disturbances, the reductions in permeability of the intact rocks decreased as the pore pressure disturbances increased, whereas the reductions increased as the disturbance amplitudes increased for the fractured rocks.

Table 5.1 Summary of the variations in permeability of the Kushiro Cretaceous sandstone

Disturbances	Intact	Fractured
Axial stress	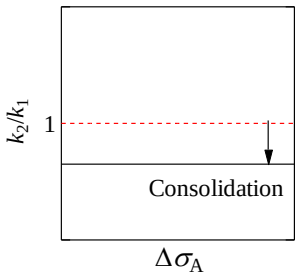	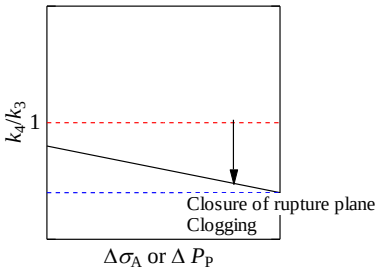
Pore pressure	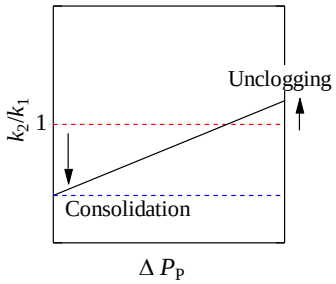	

For the case of the Shikotsu welded tuff (Table 5.2), the permeability change by the stress disturbances was small. This would be due to the large pores in this rock. These pores would not have been opened/closed or clogged/unclogged by the transient stress disturbances. The permeability decreased by fracturing. This would be due to the crushing of the glassy matrix. The crushed zone may have acted as so many water flow paths. This may be the reason why no apparent change in

permeability was shown even the some of the water flow paths closed/opened or clogged/unclogged by stress disturbances

Table 5.2 Summary of the variations in permeability of the Shikotsu welded tuff

Disturbances	Intact	Fractured
Axial stress	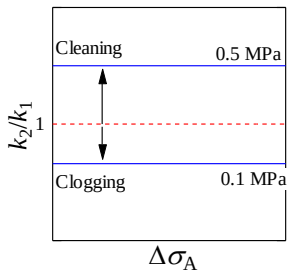	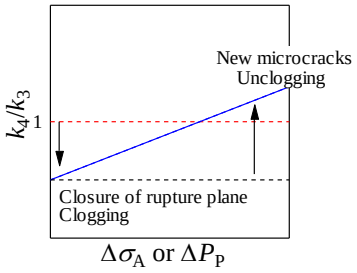
Pore pressure	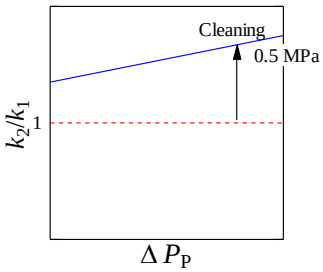	

The permeability of fractured Inada granite decreased with time in the tests. However, the permeability increased with each series of axial stress disturbances for amplitudes of 3 MPa or larger. The degree of increase in permeability increased with the axial stress disturbance amplitudes. The increased permeability decreased with time and recovered to its value before the disturbances. The time of recovery became longer for larger axial stress disturbance amplitudes.

The effects of transient stress disturbances of rock masses would be different from those of intact rocks but not so significantly different from those of fractured rocks. Considering this and also that similar effects are likely to occur for similar rock types, it is expected that the permeability of rock mass consisting of argillaceous/glassy/hard crystalline rocks may decrease/unchanged/increase owing to transient stress disturbances.

6. Concluding remarks

To clarify the effects of transient stress disturbances on rock permeability, the study of three rock types, Kushiro Cretaceous sandstone, Shikotsu welded tuff, and Inada granite were carried out. The permeability values of intact and triaxially fractured Kushirio Cretaceous sandstone and Shikotsu welded tuff were measured before and after transient axial stress or pore pressure disturbances; the permeability of triaxially fractured Inada granite was measured under multiple transient disturbances in axial stress.

The permeability of the Kushiro Cretaceous sandstone decreased at zero stress disturbances. For the intact rocks, the permeability was kept almost constant with the disturbance amplitude. For the fractured rocks, the reductions became larger as the disturbance amplitudes increased. Regarding the pore pressure disturbances, the reductions in permeability of the intact rocks decreased as the pore pressure disturbances increased, whereas the reductions increased as the disturbance amplitudes increased for the fractured rocks.

For the Shikotsu welded tuff, the permeability decreased by fracturing. However, the change by the disturbances was small for all conditions.

The permeability of fractured Inada granite decreased with time in the tests. However, the permeability increased with each series of axial stress disturbances for amplitudes of 3 MPa or larger. The degree of increase in permeability increased with the axial stress disturbance amplitudes. The increased permeability decreased with time and recovered to its value before the disturbances. The time of recovery was longer for larger axial stress disturbance amplitudes.

The stress disturbances showed either decreasing or increasing effects on the permeability depending on the rock type and experimental conditions as stated above. However, when focusing on the fractured rocks which would be more important in field applications rather than the intact rocks, the argillaceous Kushiro Cretaceous sandstone mainly exhibited decreasing effects. The effects were mainly due to the closure of the rupture planes and the clogging of flow pathways by fine particles. In contrast, the glassy Shikotsu welded tuff showed small change. This would be because there were a lot of water flow paths in crushed glassy matrix. Permeability may not change even some flow paths were opened/closed or clogged/unclogged. The crystalline Inada granite mainly exhibited increase in permeability. The effects were mainly due to the opening of the apertures propped by hard fine

particles, the enhancement of new microcracks, and unclogging of the fines from the flow pathways.

Variations in permeability due to transient stress disturbances have already been employed in seismic enhanced oil recovery (EOR) technique expecting an increase in permeability due to the movement of entrapped fluid in the reservoir. It could also be used for evaluation of the change in sealing ability of nuclear waste disposal caverns, and further employed to enhance natural gas recovery, to reroute underground water flow for various purposes, to prevent large earthquakes by inducing many small earthquakes, etc. in the future.

Further experiments on different types of rock under various conditions and consideration on the mechanisms of variations in permeability should be carried out in the future to further elucidate the effects of transient stress disturbances on rock permeability.

Acknowledgements

I would like to greatly express my sincere gratitude to Prof. Dr. Yoshiaki Fujii, my advisor, for accepting me as a doctoral student and all his generous guidance, enthusiastic encourages, suggestions and comments for this research. I am so appreciated his patient advices and all kind of supports to accomplish this research done. Not only the supervision on this research, he is such a role model for me to improve my future work behavior.

My grateful thanks to Prof. Dr. Satoru Kawasaki, Prof. Dr. Tatsuya Ishikawa, and Assoc. Prof. Dr. Jun-Ichi Kodama for being the committees of the research midterm and final defense presentations and always provided the good comments and suggestions.

I would like to extend my thanks to Assistance Prof. Dr. Diasuke Fukuda, for important advices and encouragement to improve the better research achievement. Special thanks to Mr. Takayuki Sugawara, the laboratory technician, for his kindness and all kinds of assistances during the experimental difficulties. I always could find him in every urgent inquiry.

I wish to thank to English Engineering Education Program (e^3) officers for their administrative supports.

The research could not be achieved without the support of Japan International Corporation Agency under AUN/Seed-Net program (JICA-AUN/Seed-Net) for financial support. Thanks to JICA staffs in Sapporo for warm welcoming and assistance during my stay in Hokkaido University.

Last but not least, great love and thank to my beloved family for always being care and supports. Deeply thank to my number one inspiration, my beloved mother, Bun Sok, for being everything to me.

References

Alam, B., Niiioka, M., Fujii, Y., and Fukuda, D. 2014. Effects of confining pressure on the permeability of three rock types under compression. *International Journal of Rock Mechanics and Mining Sciences*. 65. 49-61.

Bai, R. and Tien, C. 1997. Particle detachment in deep bed filtration. *Journal of Colloid and Interface Science.* 186. 307-317.

Bear, J. 1979. Hydraulics of groundwater mcgraw-hill series in water resources and environmental engineering. *New York.* 463.

Beresnev, I., Gaul, W. and Vigil, R. D. 2011. Direct pore–level observation of permeability increase in two–phase flow by shaking. *Geophysical Research Letters.* 38.

Beresnev, I. A. and Johnson, P. A. 1994. Elastic-wave stimulation of oil production: A review of methods and results. *Geophysics.* 59. 1000-1017.

Beresnev, I. A., Vigil, R. D., Li, W., Pennington, W. D., Turpening, R. M., Iassonov, P. P. and Ewing, R. P. 2005. Elastic waves push organic fluids from reservoir rock. *Geophysical Research Letters.* 32.

Bergendahl, J. and Grasso, D. 2000. Prediction of colloid detachment in a model porous media: hydrodynamics. *Chemical Engineering Science.* 55. 1523-1532.

Boeut, S., Oshima, T., Fujii, Y., Kodama, J-I., Fukuda, D., Matsumoto, H., Uchida, K. and Dassanayake, A. B. N. 2019. Variation in the permeability of intact and fractured rocks due to transient disturbances in axial stress or pore pressure. *Advances in Civil Engineering.* 2019**.** 16.

Bower, D. and Heaton, K. 1978. Response of an aquifer near ottawa to tidal forcing and the alaskan earthquake of 1964. *Canadian Journal of Earth Sciences.* 15. 331-340.

Brodsky, E. E., Roeloffs, E., Woodcock, D., Gall, I. and Manga, M. 2003. A mechanism for sustained groundwater pressure changes induced by distant earthquakes. *Journal of Geophysical Research: Solid Earth.* 108.

Candela, T., Brodsky, E. E., Marone, C. and Elsworth, D. 2014. Laboratory evidence for particle mobilization as a mechanism for permeability enhancement via dynamic stressing. *Earth and Planetary Science Letters.* 392. 279-291.

Candela, T., Brodsky, E. E., Marone, C. and Elsworth, D. 2015. Flow rate dictates permeability enhancement during fluid pressure oscillations in laboratory experiments. *Journal of Geophysical Research: Solid Earth.* 120. 2037-2055.

Doi, S. 1963. Petrological and petrochemical studies of welded tuff. *Rep. Geol. Surv. Hokkaido.* 29. 30-103.

Elkhoury, J. E., Brodsky, E. E. and Agnew, D. C. 2006. Seismic waves increase permeability. *Nature.* 441**.** 1135.

Elkhoury, J. E., Niemeijer, A., Brodsky, E. E. and Marone, C. 2010. Dynamic Stress stimulates flow in fractures: Laboratory observations of permeability enhancement. *Journal of Geophysical Research.* 115.

Elkhoury, J. E., Niemeijer, A., Brodsky, E. E. and Marone, C. 2011. Laboratory observations of permeability enhancement by fluid pressure oscillation of in situ fractured rock. *Journal of Geophysical Research: Solid Earth.* 116.

Fujii, Y., Ichihara, Y., Matsumoto, H., Kodama, J-I., Fukuda, D. and Dassanayake, A. B. 2018a. Water drainage from kushiro coal mine decreased on the day of all m ≥ 7.5 earthquakes and increased thereafter. *Scientific Reports.* 8. 16472.

Fujii, Y., Ishijima, Y., Ichihara, Y., Kiyama, T., Kumakura, S., Takada, M., Sugawara, T., Narita, T., Kodama, J-I. and Sawada, M. 2011. Mechanical properties of abandoned and closed roadways in the Kushiro Coal Mine, Japan. *International Journal of Rock Mechanics and Mining Sciences.* 48. 585-596.

Fujii, Y., Sheshpari, M., Kodama, J-I., Fukuda, D. and Dassanayake, A. B. 2018b. Prevention of catastrophic volcanic eruptions, large earthquakes underneath big cities, and giant earthquakes at subduction zones. *Sustainability.* 10. 1908.

Fujii, Y., Yamada, M., Fukuda, D. and Kodama, J-I. Prevention of giant earthquakes by underground nuclear explosions. Spring Meetingof MMIJ, 2017. The Mining and Materials Processing Institute of Japan. 3411-17-07.

Gudmundsson, A. 2000. Active fault zones and groundwater flow. *Geophysical Research Letter.* 27. 2993-2996.

Jónsson, S., Segall, P., Pedersen, R. and Björnsson, G. 2003. Post-earthquake ground movements

correlated to pore-pressure transients. *Nature.* 424. 179.

Kitagawa, Y., Koizumi, N., Takahashi, M., Matsumoto, N. and Sato, T. 2006. Changes in groundwater levels or pressures associated with the 2004 earthquake off the west coast of northern Sumatra (M9. 0). *Earth, Planets and Space.* 58. 173-179.

Lai, G., Jiang, C., Han, L., Sheng, S. and Ma, Y. 2016. Co-seismic water level changes in response to multiple large earthquakes at the lgh well in sichuan, China. *Tectonophysics.* 679. 211-217.

Lin, W., Kwaśniewski, M., Imamura, T. and Matsuki, K. 2006. Determination of three-dimensional in situ stresses from anelastic strain recovery measurement of cores at great depth. *Tectonophysics.* 426. 221-238.

Lin, W. and Takahashi, M. 2008. Anisotropy of strength and deformation of inada granite under uniaxial tension. *Journal of Rock Mech Engineering.* 27.

Liu, W. and Manga, M. 2009. Changes in permeability caused by dynamic stresses in fractured sandstone. *Geophysical Research Letters.* 36.

Manga, M., Beresnev, I., Brodsky, E. E., Elkhoury, J. E., Elsworth, D., Ingebritsen, S., Mays, D. C. and Wang, C.Y. 2012. Changes in permeability caused by transient stresses: field observations, experiments, and mechanisms. *Reviews of Geophysics.* 50.

Manga, M. and Wang, C. 2015. 4.12. Earthquake hydrology. *Treatise on Geophysics, Second Edition. Elsevier. Oxford***.** 305-328.

Matsuki, K. and Takeuchi, K. 1993. Three-dimensional In situ stress determination by anelastic strain recovery of a rock core. *International Journal of Rock Mechanics and Mining Sciences & Geomechanics Abstracts. Elsevier*. 1019-1022.

Matsumoto, H., Uchida, K., Takahashi, T., Fujii, Y., Kodama, J. and Ayizawa, J. 2014. 2nd Report of activity of rock formation gas exploration subcommittee. *Proc. Mmij2014 (Kumamoto),* Japan.

Oda, M., Takemura, T. and Aoki, T. 2002. Damage growth and permeability change in triaxial compression tests of inada granite. *Mechanics of Materials.* 34. 313-331.

Orihara, Y., Kamogawa, M. and Nagao, T. 2014. Preseismic changes of the level and temperature of confined groundwater related to the 2011 Tohoku earthquake. *Scientific Reports.* 4. 6907.

Pride, S. R., Flekkøy, E. G. and Aursjø, O. 2008. Seismic stimulation for enhanced oil recovery. *Geophysics.* 73. 023-035.

Roberts, P. M. 2005. Laboratory observations of altered porous fluid flow behavior in berea sandstone induced by low-frequency dynamic stress stimulation. *Acoustical Physics*. 51. S140-S148.

Roberts, P. M., Esipov, I. B. and Majer, E. L. 2003. Elastic wave stimulation of oil reservoirs: promising EOR technology?. *The Leading Edge*. 22. 448-453.

Roeloffs, E. A. 1998. Persistent water level changes in a well near parkfield, california, due to local and distant earthquakes. *Journal of Geophysical Research: Solid Earth*. 103. 869-889.

Saroglou, C. and Kallimogiannis, V. 2017. Fracturing process and effect of fracturing degree on wave velocity of a crystalline rock. *Journal of Rock Mechanics and Geotechnical Engineering*. 9. 797-806.

Shmonov, V., Vitovtova, V. and Zharikov, A. 1999. Experimental study of seismic oscillation effect on rock permeability under high temperature and pressure. *International Journal of Rock Mechanics and Mining Sciences and Geomechanics Abstracts*. 405-412.

Wang, C.Y. and Manga, M. 2009. *Earthquakes and water.* Springer.

Wang, C.Y. and Chia, Y. 2008. Mechanism of water level changes during earthquakes: near field versus intermediate field. *Geophysical Research Letters*. 35.

Wang, G., Mitchell, T., Meredith, P., Nara, Y. and Wu, Z. 2016. Influence of gouge thickness and grain size on permeability of macrofractured basalt. *Journal of Geophysical Research: Solid Earth.* 121. 8472-8487.

Xing, Z-G., He, Y., Du, W. and Fang, J. 2018. Review of research process and application of acoustic wave testing technology for rock. *IOP Conference Series: Earth and Environmental Science. IOP Publishing*. 052045.